Evolution of a hydrocarbon migration pathway along basin-bounding faults: Evidence from fault cement

James R. Boles, Peter Eichhubl, Grant Garven, and Jim Chen

ABSTRACT

Extensive calcite fault cement has resulted from leakage of Santa Barbara basin fluids and hydrocarbons into the Refugio-Carneros fault, a north-bounding structure to the basin. Calcite cements are only found at the end segments of the 24-km (15-mi)-long fault zone, which has less than 150 m (490 ft) of maximum normal offset. The calcite is contemporaneous with fault movement, as evidenced by pervasive crystal twinning and brecciation, as well as textures indicating repeated episodes of rapid fluid flow and calcite cementation. Based on U-Th dates of the calcite, fluid flow along the fault occurred between 110 and greater than 500 ka, indicating that fluid migration was intermittently active during the recent uplift history of the basin flank. Stable carbon isotopic values of the calcite are $\delta^{13}C_{PDB} = -35$ to -41 ‰, which means that the carbon source is predominantly thermogenic methane. The composition of fluid inclusions in calcite is consistent with mixing of meteoric and saline water in the presence of liquid and gaseous hydrocarbons. Fluid-inclusion homogenization temperatures of about 80–95°C suggest that hot water leaked from 2- to 3-km (1.2- to 1.9-mi) depths in the basin and moved up faults on the basin flank at rates rapid enough to transport substantial heat to shallow depths. Finite-element models show that, in this case, this process requires faulting of an overpressured basin and that a single flow event would have lasted for at least 10^3 yr.

Subsurface fluid pressures at comparable depths in the offshore section today are close to hydrostatic, and therefore, only slow hydrocarbon seepage occurs. When combined with the U-Th age data, this suggests that over a 10^5-yr timescale, basin fluid flow has evolved from the rapid expulsion of hot water and gas being carried up along active, bounding faults derived from overpressured strata to present hydrostatic conditions of slow, buoyancy-driven seepage of hydrocarbons.

Manuscript received April 24, 2003; provisional acceptance August 27, 2003; revised manuscript received December 16, 2003; final acceptance February 9, 2004.

AUTHORS

JAMES R. BOLES ~ *Department of Geological Sciences, University of California, Santa Barbara, California, 93106; boles@geol.ucsb.edu*

James Boles is a professor of geology at the University of California at Santa Barbara. His B.S. degree is from Purdue, his M.S. degree is from the University of Wyoming, and his Ph.D. is from the University of Otago (New Zealand). He has conducted research on various aspects of clastic diagenesis for more than 35 years. His current research is on fault diagenesis, pressure solution, and geochemical tools for interpreting diagenetic processes.

PETER EICHHUBL ~ *Department of Geological and Environmental Sciences, Stanford University, Stanford, California, 94305-2115*

Peter Eichhubl (Ph.D., University of California, Santa Barbara, 1997) is a research associate affiliated with the Stanford Rock Fracture Project. His research interests include fault and fracture mechanics, deformation processes in sediment and sedimentary rock, fluid flow in sedimentary basins, and the chemical interaction of rock and pore fluid.

GRANT GARVEN ~ *Department of Earth and Planetary Sciences, Johns Hopkins University, Baltimore, Maryland, 21218-2687*

Grant Garven is a professor of hydrogeology at Johns Hopkins University and founding coeditor of the new journal *Geofluids*. His research focuses on the paleohydrology of sedimentary basins and the application of reactive fluid-flow modeling for understanding processes of diagenesis, hydrothermal ore formation, and poroelastic deformation.

JIM CHEN ~ *Division of Geological and Planetary Sciences, California Institute of Technology, Pasadena, California, 91125*

James Chen (Ph.D., University of California, Santa Barbara, 1977) is a research scientist affiliated with the Jet Propulsion Laboratory, Caltech. His research interests include investigating various aspects of isotope geochemistry, geochronology, and cosmochemistry using both long-lived and short-lived radioactive nuclei.

ACKNOWLEDGEMENTS

Mark Grivetti first pointed out the westerly calcite outcrops to the senior author, and he and Bill Tracy participated in some of the early field work. University of California, Santa Barbara, undergraduate students Tom Carpenter and Tom Neely provided helpful field assistance. Karen Christensen, Venoco, kindly provided an interpreted offshore structural cross section. Stacey Zeck-Boles read and greatly improved early versions of the paper. We gratefully acknowledge the Department of Energy Basic Research funding for this project (Boles/Garven DOE 444033-22433). P. Eichhubl acknowledges support through the Stanford Rock Fracture Project.

INTRODUCTION

Hydrocarbon migration pathways are important components of hydrocarbon systems (Magoon and Dow, 1994; Losh et al., 1999; Aydin, 2000), and if pathways extend to the surface, they may contribute to greenhouse gas and influence global climate (MacDonald, 1990; Nisbet, 1990; Kennett et al., 2002). Modern surface seeps can be the manifestation of major structurally controlled subsurface hydrocarbon migration pathways (e.g., Wilson et al., 1974; Hornafius et al., 1999; Tryon et al., 1999; Eichhubl et al., 2000). Hydrocarbon migration pathways are becoming increasingly recognized in the geologic record from application of geochemical tools, as well as fluid inclusions in cements (e.g., Hathaway and Degens, 1969; Sample et al., 1993; Chan et al., 2000; Eichhubl and Boles, 2000a, b; Budai et al., 2002). The isotopically light carbon in calcite cement (commonly with $\delta^{13}C_{PDB}$ of $-20‰$ or less) is the prime geochemical evidence for the former presence of methane, because it represents carbon derived from oxidation of methane (e.g., Donovan et al., 1974; see review in Jørgensen, 1992; Schumacher, 1996). The association of light carbon isotopes with hydrocarbon fluid inclusions suggests ancient hydrocarbon pathways. In many cases, this geochemical evidence is found above leaking hydrocarbon reservoirs. In some cases, bacterially generated soil methane may also be oxidized to form CO_2 and calcite (Quade et al., 1989), but these are not associated with liquid hydrocarbon inclusions.

In this paper, extensive calcite deposits filling a fault zone are described, in which the calcite carbon is derived from oxidation of methane (Boles and Grivetti, 2000). These deposits resulted from high-temperature fluids, including both liquid and gaseous hydrocarbons, derived from a probable overpressured basin. The fluids were focused up a fault zone to the surface where they mixed with oxygenated meteoric water. Our study, when viewed in conjunction with modern offshore, cold hydrocarbon seeps in the Santa Barbara Channel (Fischer and Stevenson, 1973; Hornafius et al., 1999; Eichhubl et al., 2000), creates a picture of how hydrocarbon migration has evolved through time at a basin margin as the pore-fluid pressure at depth has dissipated.

GEOLOGIC FRAMEWORK

Tectonic and Hydrocarbon Setting

The Santa Barbara coastal area was a site of largely marine sedimentation that extended from the Cretaceous until late Pleistocene (Ingle, 1980). During this time, the area was undergoing plate convergence and, beginning after the Oligocene, transpression resulted in crustal rotation and the opening of subbasins (Atwater, 1970; Hornafius et al., 1986). Beginning in the Pliocene, the east-west–trending Santa Ynez Mountains, bounded to the north by the Santa Ynez

fault (Figure 1a) (Dibblee, 1966), was uplifted along the margin of the Santa Barbara basin (Jackson and Yeats, 1982). This uplift and deformation created several secondary fault systems, including the Refugio-Carneros fault, which roughly parallel the coastline in the Santa Ynez Mountains (Figure 1a). Offshore burial of sediment was sufficiently deep that hydrocarbons were generated, chiefly from the Miocene Monterey Formation, an organic-rich siliceous mudstone deposited as a result of coastal upwelling (Ogle et al., 1987). Fractured siliceous mudstone and dolomite of the Monterey Formation are also the main reservoir for offshore oil production in the Santa Barbara Channel.

Hydrocarbon accumulations in the area adjacent to the Refugio-Carneros fault include the now abandoned onshore Refugio Cove Gas, Capitan Oil, Ellwood Onshore/Offshore Oil, La Goleta Gas, and Mesa Oil fields (Figure 1a; Table 1). Today, offshore production in the area includes the South Ellwood anticline producing from Platform Holly, the Molino offshore gas accumulation (under development), and the Hondo structure currently being produced from Platforms Hondo and Harmony. In general, formation waters of onshore oil fields have lower salinity values compared to offshore fields because of the dilution of original trapped marine water by meteoric recharge from the mountains (Table 1). This paper will demonstrate that the calcite deposits in the Refugio-Carneros fault reflect the mixing of offshore and meteoric fluids, with hydrocarbons derived from offshore accumulations and meteoric fluids providing a source of oxygen for oxidation of methane.

Refugio-Carneros Fault

The Refugio-Carneros fault is one of several east-west–to northwest-southeast–trending faults in the Santa Barbara coastal area, including the Dos Pueblos, Eagle, Glen Annie, More Ranch, San Pedro, and San Jose faults and the major Santa Ynez fault (Figure 1a) (Dibblee, 1987a, b; 1988, U.S. Geological Survey, unpublished work). These faults cut strata of Miocene and younger age and are believed to be part of the regional transpressive deformation and clockwise rotation that has occurred along the Pacific and North American plate junction since the Miocene (Nicholson et al., 1994).

The Refugio-Carneros fault (Figure 1a) is 24 km (15 mi) long, strikes approximately east-west roughly parallel to bedding, and dips 35–60° north. Fault offsets of formation contacts on several ridge tops and sides of steep canyons indicate as much as 120 m (390 ft) of normal slip. Although well defined on a 1:24,000 map scale (Dibblee, 1987a, b; 1988), most of the fault outcrops are covered with brush, with exposure limited to cemented portions of the fault and of its damage zone. In the western part, the fault strikes N75°W (Figures 1b, c; 2) and cuts Miocene Vaqueros sandstone and Rincon formation shale (Dibblee, 1988). The eastern section is within Vaqueros sandstone. The eastern end of the fault is poorly exposed because of Quaternary cover, but an east-west–oriented set of steeply dipping, carbonate-cemented veins in Vaqueros sandstone can be found in a gully approximately 600 m (1970 ft) north of the projected trace of the Refugio-Carneros fault (Figure 1a) as mapped by Dibblee (1987a). We interpret this isolated exposure as marking an eastern segment of the Refugio-Carneros fault.

FAULT ZONE MINERALIZATION

Distribution and Morphology of Fault Cement

Coarsely crystalline calcite fault cement, as much as 1.5 m (5 ft) thick, is only found along the western and eastern parts of the fault. Calcite cement has not been found in the fault along the central part, despite the fact that the fault trace is exposed in numerous canyons and hilltops.

Along the westernmost 1.5-km (1-mi)-long section of the fault, calcite cements occur as discontinuous tabular bodies as much as 1.5 m (5 ft) thick (Figure 1a, b locations A–F). The largest exposure of fault cement (Rancho Tajiguas at N34°29.469′, W120°5.333′) is about 200 m (660 ft) from the western termination of the fault, forming a tabular body of calcite at least 1.5 × 15 × 15 m (5 × 50 × 50 ft) in size or about 338 m^3 (11,900 ft^3) (Figure 1b, location A). The tabular bodies are parallel to the strike of the fault, which dips north at 35–60° (Figure 3a). The main fault is consistently on the north side of the calcite bodies, forming striated and polished slip surfaces (Figure 1b). At one of the calcite outcrops (Figures 1b, location E; 3b), slickensides rake 20°E on the main fault surface, indicating a predominant strike-slip component. Veins with predominant opening mode, varying in thickness from a few millimeters to more than 10 cm (4 in.), extend into the sandstone host rock at this and several other locations. These veins are oriented at an oblique angle to the main trace (Figure 3b) that is consistent with splay crack geometry resulting from a left-lateral strike-slip component on the Refugio-Carneros fault.

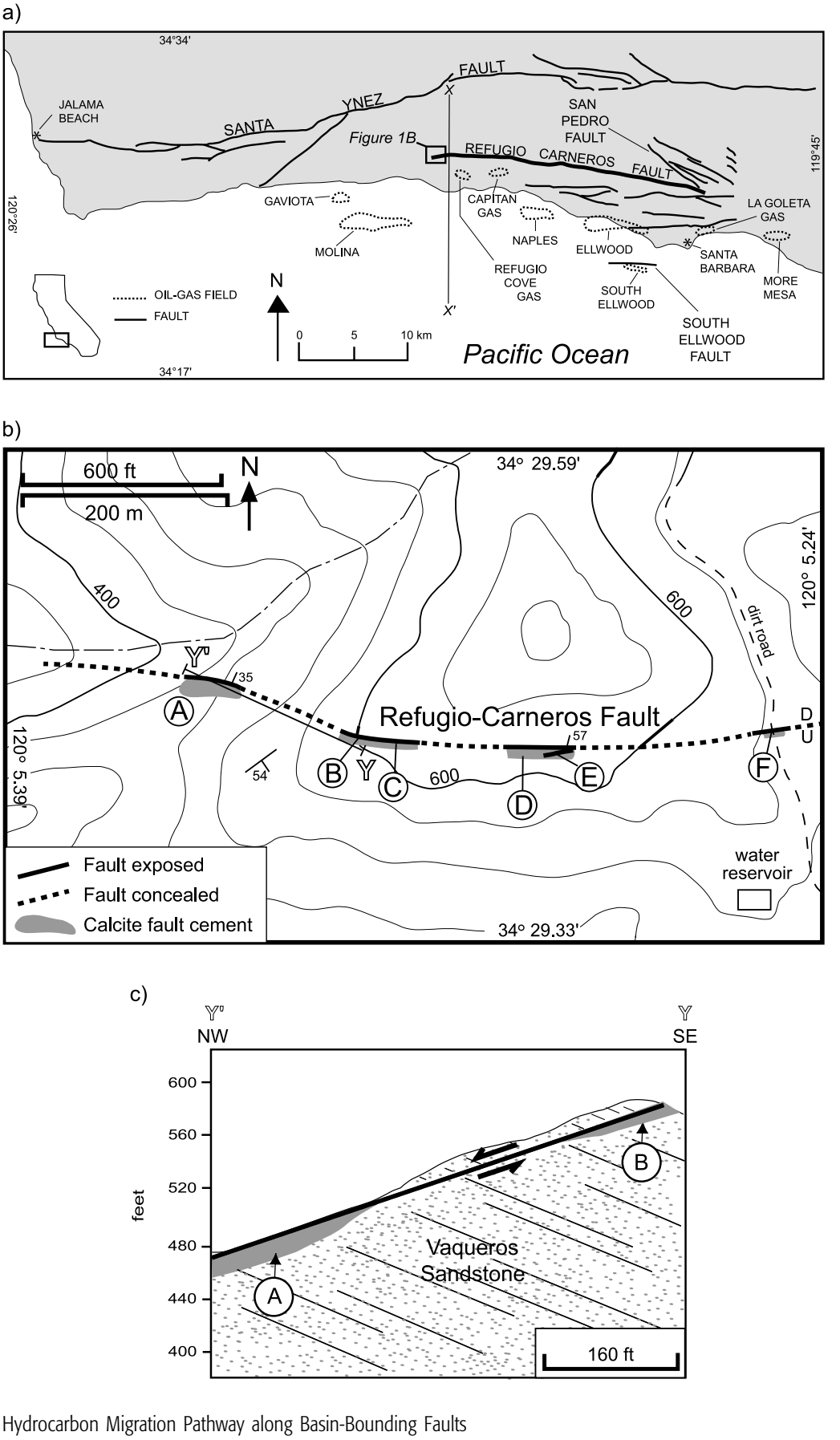

Figure 1. (a) Location of Refugio-Carneros fault, Santa Ynez fault and oil and gas fields in the vicinity of Santa Barbara, California. (b) Field map of fault calcite localities near the western end of Refugio-Carneros fault. Topographic contour interval is 40 ft. Locality A = 1.5 × 15 × 15 m (5 × 49 × 49 ft) coarse blocky and brecciated calcite slab; B = blocky and brecciated calcite, 1.7 m (5.6 ft) thick, with hematite alteration; C = blocky calcite with acicular crystal spray remnant; D = coarse blocky calcite, 1 × 1.75 × 1 m (3.3 × 5.7 × 3.3 ft) float block; E = blocky and brecciated calcite with polished slip surface 1 × 2.5 × 5 m (3.3 × 8 × 16 ft); F = blocky coarse calcite 0.5 m (1.6 ft) thick (exposed on dirt road). (c) Cross section YY′ from (b).

Table 1. Hydrocarbon Production and Subsurface Water Composition in the Vicinity of the Refugio-Carneros Fault*

Sample location	Formation	Depth (m)	Water Temperature (°C)	Water Salinity (TDS)	Water Isotopic SMOW (‰)	Sulfate Concentration (mg/L)	Magnesium Concentration (mg/L)
Onshore Fields							
Refugio Cove gas field	Vaqueros	460	nd	800	nd	nd	nd
	Sespe	880	49	2054	nd	nd	nd
Capitan oil field	Vaqueros (onshore)	335	37	4227	nd	nd	nd
	Sespe	840	49	7630	nd	nd	nd
La Goleta gas field	Vaqueros	1204	63	3950	nd	nd	nd
Ellwood onshore	Rincon	792	nd	34,240	nd	nd	nd
	Vaqueros	1036	68	20,544	nd	nd	nd
	Upper Sespe	1128	nd	17,120	nd	nd	nd
	Bell 14	1463	nd	17,120	nd	nd	nd
Mesa oil field	Vaqueros	655	nd	19,000	nd	95	nd
Offshore Fields							
Naples offshore	Vaqueros	2700	nd	10,200	nd	nd	nd
Capitan oil field	Vaqueros (offshore)	nd	nd	20,544	nd	nd	nd
Molina South Ellwood-Platform Holly (average of 4)	Monterey	1030	58	31,200	2.34	82	31
Platform Hondo (average of 6)		>1000	nd	30,654	4.76	136	34
Average seawater				35,000	0	2712	1029
Well water (Taijugas Ranch area)	Vaqueros	90	nd	1400	nd	460	10
Tunnel seep water (Santa Barbara Mission Tunnel)	Vaqueros	70	15	<1000	−6.8	440	42

*Oil field-producing data from California Division of Oil and Gas Publication. Oil field water isotopic analyses from Eichhubl and Boles (1998). Sulfate and magnesium analyses from unpublished data of J. Boles and P. Eichhubl. Well-water data from unpublished water-quality analysis. Mission Tunnel water analyses from Rademacher et al. (2003). nd = not determined.

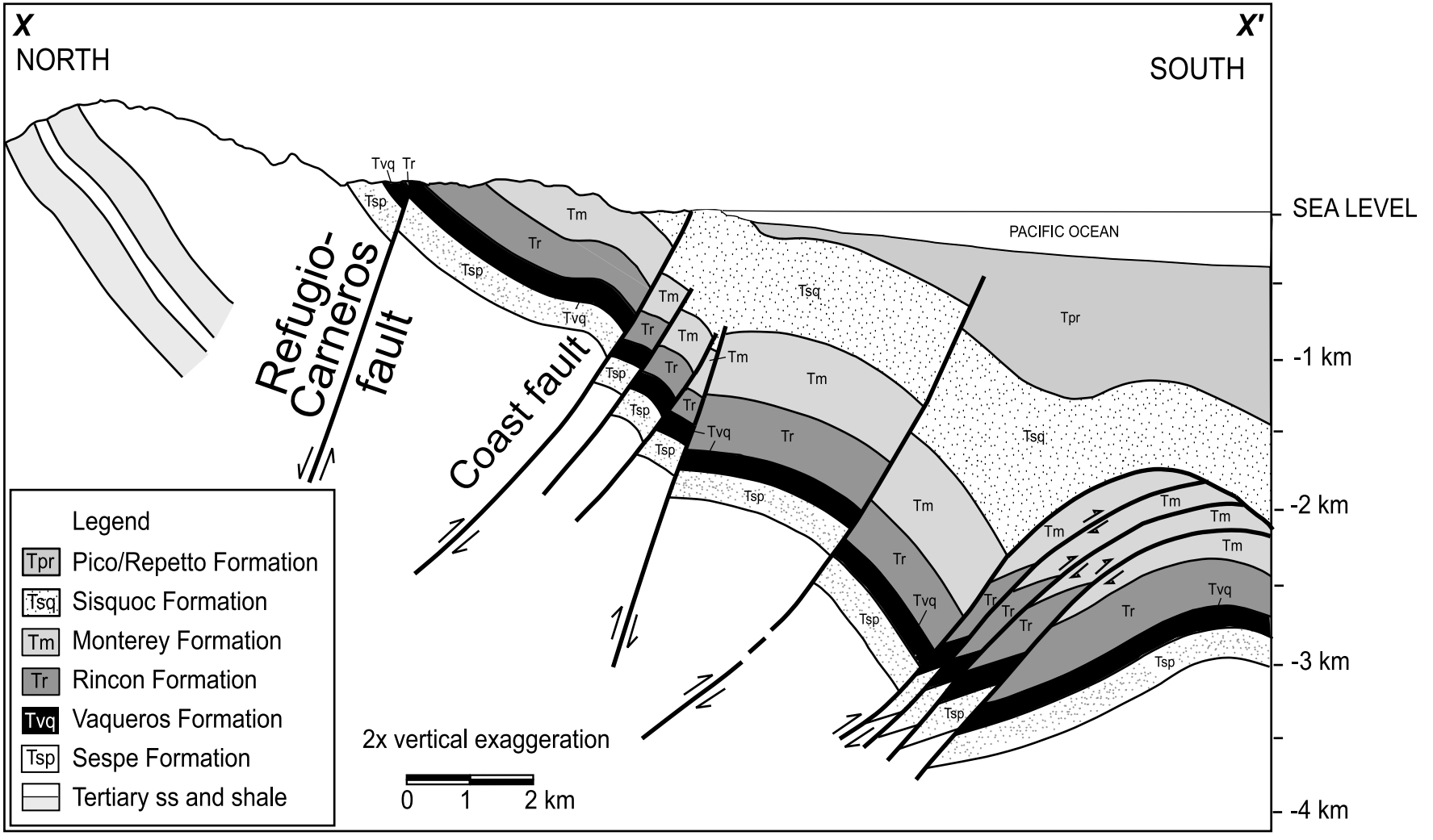

Figure 2. North-south cross section across western segment of the Refugio-Carneros fault. See Figure 1a for location of cross section line. Onshore geology is from Dibblee (1988). Offshore geology interpreted by Karen Christensen (Venoco, Inc.) from offshore seismic data.

At the eastern part of the Refugio-Carneros fault, calcite occurs in a 4-m (13-ft)-long ravine exposure perpendicular to the fault trend at N34°27.698′, W119°49.567′. At this locality, calcite occurs in a series of subparallel veins 1–30 cm (0.4–12 in.) thick and separated by sandstone matrix. The sequence of veins is about 2 m (7 ft) thick and dips 80° north, parallel to bedding. The fault is not exposed in the ravine, but float of thick calcite vein cement (>20 cm [>8 in.] thick) on the north end of the exposure suggests the fault is a few meters to the north.

At both the eastern and western parts of the fault, some calcite forms radiating sprays of acicular crystals, as much as 10 cm (4 in.) long, which have nucleated on the walls of veins and grown inward (Figure 3c). The growth of the crystals into open fracture space suggests that the rate of fracture opening outpaced the rate of cement precipitation. These crystal sprays are most common at the eastern locality. The acicular crystals appear to be replaced in most locations by blocky calcite (Figure 3d). The blocky crystals range in size from a few millimeters to 7 cm (3 in.) and have multiple sets of twin lamellae (Figure 3e). Blocky calcite is commonly brecciated because of shearing along slip surfaces that are contained in the cement bodies and that are subparallel to the strike of the fault (Figure 3f).

A float sample, collected 1.2 km (0.7 mi) from the western fault termination on Rancho Agua Ito (N34°28.476′, W120°04.410′), consists of millimeter-thick calcite bands (Figure 3g). In thin section, the bands are composed of radiating crystal sets with euhedral terminations. Heavy minerals and quartz sand grains are trapped on the growth faces along the bands (Figure 3h). We interpret these detrital layers to reflect episodic pulses of rapid fluid flow and sand-particle entrainment. Intervening periods of slower fluid flow resulted in precipitation of detritus-free cement layers.

The contact to the calcite-filled veins in several examples contains a diffuse zone with as much as 30–40% sand grains cemented by calcite as determined by point counting (Figure 3i). In comparison, the sandstone country rock has about 70% sand grains with 30% calcite cement. In Figure 3i, the detrital micas in the country rock are oriented roughly perpendicular to the vein wall, parallel to bedding, whereas in the diffuse zone, the micas are oriented subparallel to the vein wall. The micas in the diffuse zone appear to have been reoriented from fluid flow or shearing, although the calcite in the diffuse zone does not show evidence of shearing. The reorientation of micas suggests that the sand was eroded from the vein walls during rapid flow events, and that grains were realigned parallel to flow. As will be shown in the subsequent discussion, these thin veins have a different isotopic composition than the calcite in the main fault.

Iron oxide, predominantly hematite, is relatively common in sandstone adjacent to the fault (Figure 3j). Hematite occurs as a red alteration product after detrital lithic sand grains, and as grain rim and pore-filling patches of hematite cement. In some cases, hematite also occurs in the calcite vein fill, where it rims pseudomorphs of preexisting crystals and follows fractures. Sandstones sampled away from the fault typically have minor pyrite cement, and hematite is sparse. The presence of hematite suggests highly oxidizing conditions associated with fluids in the fault zone. The source of iron in hematite (Fe_2O_3) is likely from oxidation of pyrite (FeS_2).

U-Th Age of Calcite Mineralization

Eleven samples of calcite fault cement were dated using the U-Th technique. Details on the technique and a detailed analysis of these results will be described in a separate paper. Blocky carbonate has uranium concentrations ranging from 3.8 to 456 ppb, and thorium concentrations from 0.17 to 36.8 ppb. All samples display large ^{238}U-^{234}U disequilibrium, with activity ratios ranging from 1.06 to 1.39, exhibiting large excess of ^{234}U. Five samples yield apparent U-Th ages ranging from 107 to 420 ka. Six other samples yield ages greater than 500 ka, which are outside of the useful range of this dating technique (Faure, 1986). Relatively old and young ages are found at both end segments of the fault, suggesting fluid movement did not progress from one end to the other.

These ages reflect the final crystallization of the calcite that may have undergone multiple stages of dissolution and precipitation. Therefore, the dates are minimum ages of the fluid flow that resulted in calcite precipitation. Because the calcite fills fault-related openings, it postdates the initiation of faulting. Furthermore, the calcite in the dated samples is twinned and brecciated, which means that it predates the last fault movement. Therefore, the age of the calcite vein fill is within the span of fault activity. These results indicate that the Refugio-Carneros fault is relatively young (Pleistocene), and that it was active for at least several hundred thousand years.

Calcite Fluid Inclusions

Fluid-inclusion heating and freezing experiments were performed on three calcite samples to obtain information

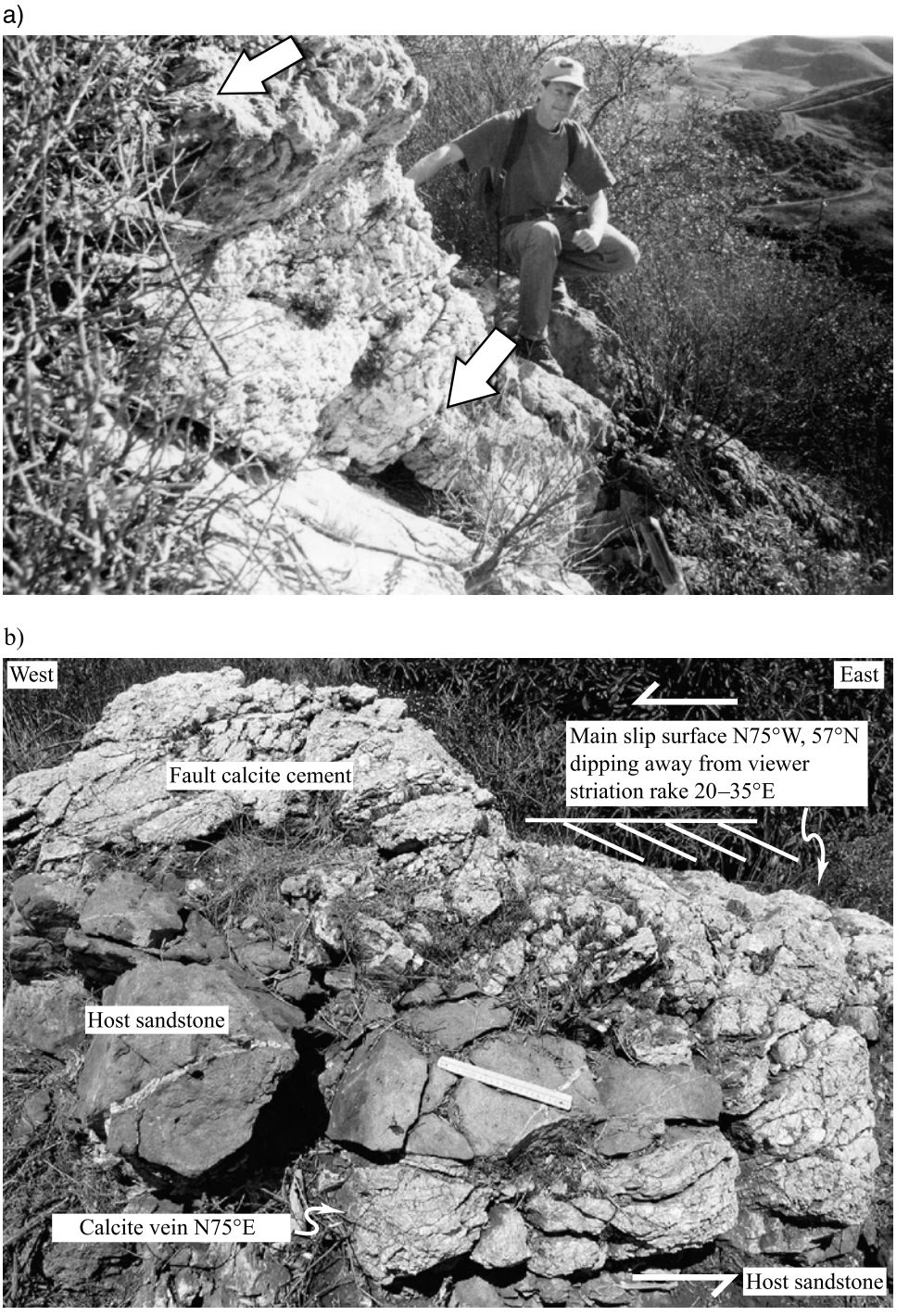

Figure 3. Occurrence of fault cements. (a) Field geologist showing solid mass of calcite in north (left)-dipping fault zone. Arrows show boundaries of calcite fault zone. Location B, Figure 1b. (b) Sandstone sliver contained between the blocky calcite fault cement and a calcite-cemented vein extending into the host sandstone at an oblique angle. The oblique vein orientation suggests a left-lateral strike-slip component for the Refugio-Carneros fault at this location. Location E, Figure 1b. White ruler is 20 cm (8 in.) long.

about temperature and fluid composition at the time of cement precipitation (Table 2). There are numerous single-phase aqueous inclusions and less common primary two-phase inclusions. Two-phase inclusions have homogenization temperatures ranging from around 80 to in excess of 100°C (Table 2). Salinities, as determined from melting temperatures of previously frozen inclusions, are highly variable, with some samples having relatively freshwater inclusions (0.3 wt.% NaCl equivalent), and others having salinities similar to seawater (3.5 wt.% NaCl equivalent). There is no correlation between salinity and homogenization temperature in this limited data set (Figure 4). Finally, liquid hydrocarbon inclusions are present in one of the samples.

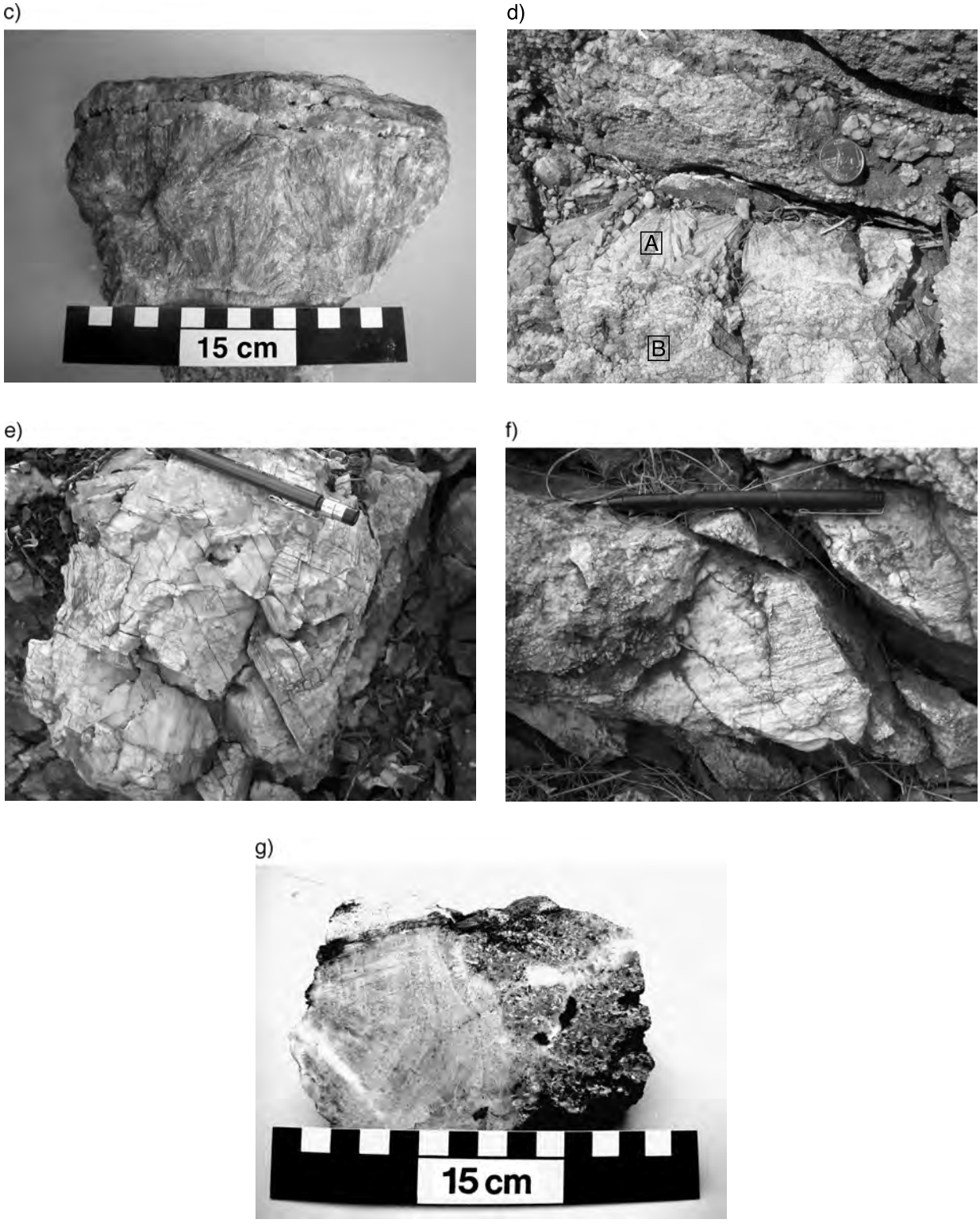

Figure 3. Continued. (c) Acicular calcite sprays growing into fault fracture space. Sample from ravine locality, eastern segment of fault. (d) Acicular crystals of calcite (A) partially recrystallized to blocky calcite (B). Photo from locality C, Figure 1b. Coin (2.5 cm; 1 in.) rests on host sandstone. (e) Large 10-cm (4-in.)-scale, blocky, calcite crystals with twin lamellae. Sample from location A, Figure 1b. Pencil is 15 cm (6 in.) long. (f) Brecciated outcrop showing a striated slip surface. Calcite breccia clasts have multiple finely twinned lamella. Photo from location E, Figure 1b. Pencil is 15 cm (6 in.) long. (g) Calcite fault cement from western part of fault with multiple growth bands. Right side of sample is sandstone host rock. Sample from Rancho Agua Ito at N34°28.476′, W120°04.410′.

h)

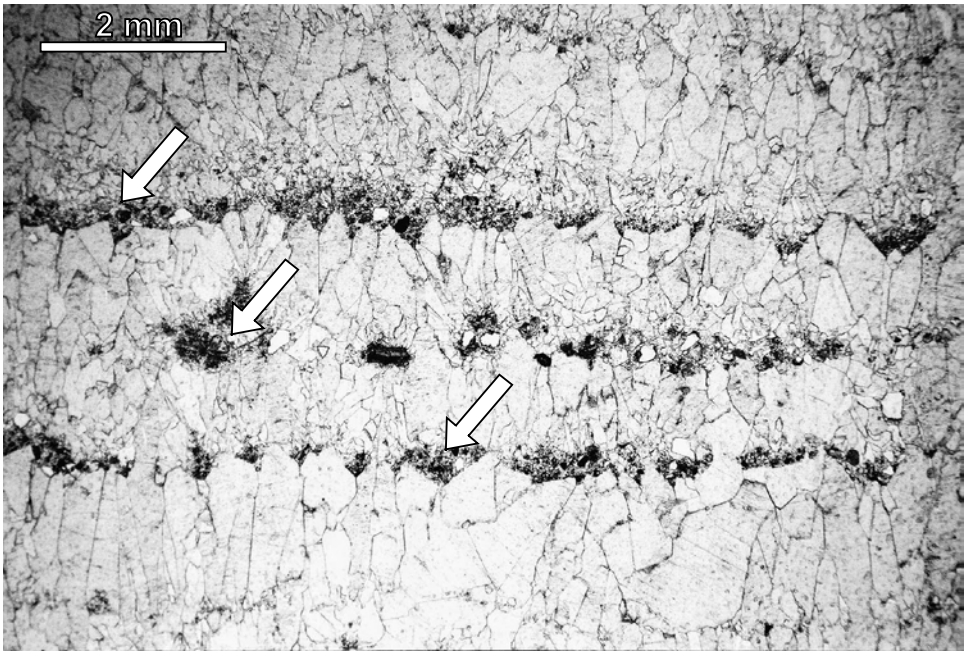

Figure 3. Continued. (h) Photomicrograph of (g) showing growth bands with euhedral crystal terminations overlain by concentrations of detrital minerals (arrows). Plain light.

Most of these hydrocarbon inclusions have pale yellow ultraviolet fluorescence, with a few having a blue fluorescence.

Oxygen and Carbon Isotopic Composition of Calcite

Calcite vein and fault cement was sampled using a dental drill with a 1-mm (0.04-in.)-diameter tip. A few samples are acid extracts from calcite-cemented sandstone adjacent to the fault zone. Several of the acicular calcites were analyzed along their length to check for composition changes with growth. Suites of samples were also analyzed across the fault zone, perpendicular to the fault strike, to look for composition trends at the outcrop scale.

Calcite from the main fault zone has a relatively narrow range of oxygen isotopic composition between −9.5 and −11 ‰ (Peedee belemnite, PDB) and carbon isotopic compositions between −40 and −30 ‰ (PDB) (Table 3; Figure 5). Heavy carbon values are from cements in the sandstone matrix (analyses 28–33 of Table 3; Figure 5). There is no systematic difference between acicular and blocky calcite, indicating that they both have formed at similar conditions. The lightest carbon isotopic values (−40 to −42 ‰, analyses 9, 10, 13, 26, and 27 of Table 3) are commonly associated with the relatively coarse, blocky crystals near the boundaries of the fault zones.

Analyses of calcite from closely spaced samples (millimeter scale) of the banded calcite (Figure 3g) have relatively uniform isotopic compositions (analyses 16–25 of Table 3), varying by only 3 ‰ in carbon and 0.5 ‰ in oxygen. Assuming these layers represent distinct fluid-flow events, each pulse appears to have had approximately the same composition as the preceding one, at least on the 1-mm (0.04-in.) sampling scale. The acicular crystals at the eastern part of the fault (analyses 46–75 of Table 3) likewise show very little variation in isotopic composition along their 70-mm (2.7-in.) length.

The heavier oxygen isotopic composition of the sandstone cement relative to the calcite in the main fault is consistent with cooling of the fluid in the sandstone matrix adjacent to the main fault. The heavier carbon isotopic composition of the sandstone matrix as well as some of the thin veins relative to the calcite values in the main fault calcite could be explained by dissolution of locally abundant calcite tests of marine fossils from the sandstone.

Strontium Isotopic Composition of Calcite

Strontium isotopic ratios of two samples from the western part of the fault (same samples as analyses 12 and 26 of Table 3) have strontium isotopic values of 0.709272 (±17) and 0.709433 (±16), respectively

i)

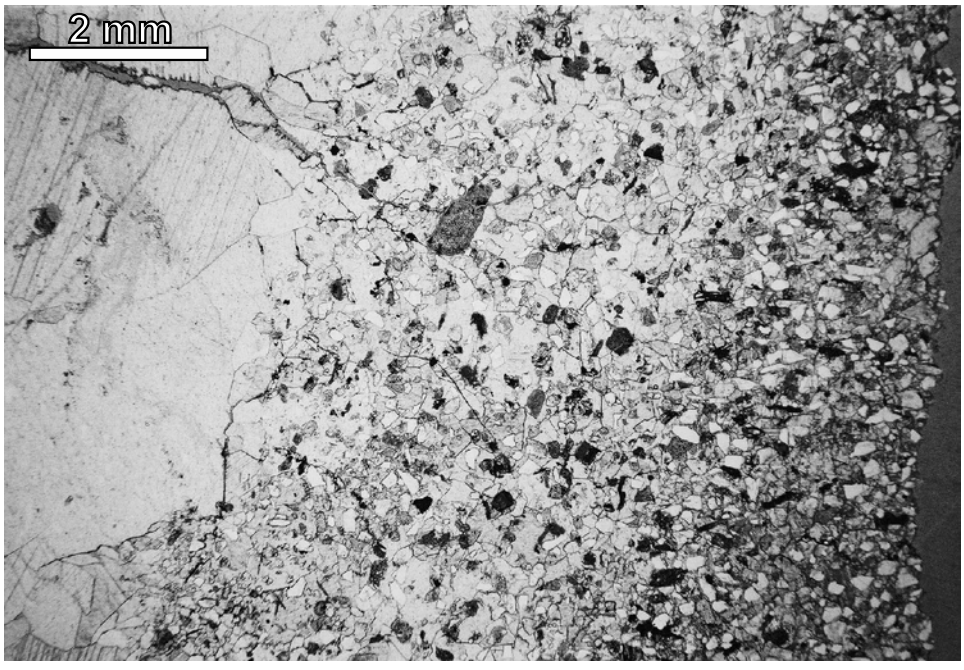

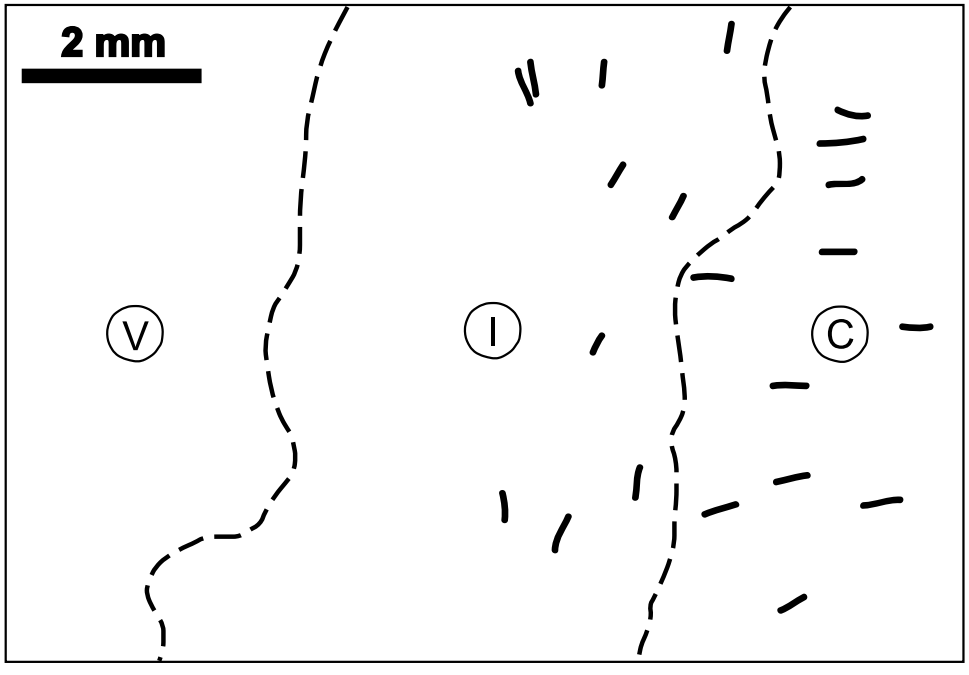

Figure 3. Continued. (i) Photomicrograph of thin vein from ravine locality at eastern part of fault with diffuse boundary zone (I) with 70% cement separating vein (V) from country rock (C) with 30% cement. Detrital micas (dark elongate grains) are oriented subparallel to the walls of the main vein in the diffuse zone, whereas micas in the country rock are mostly perpendicular to the vein and parallel to bedding. Plain light.

(standard errors in parenthesis, analyses by J. Bryce in the laboratory of J. Mattinson, University of California at Santa Barbara, values relative to National Bureau Standards (NBS) 987 = 0.71024). The second value is significantly higher than modern seawater, which has a value of about 0.7092 (DePaolo and Ingram, 1985). The Sr content of the fault calcite is very low (0.001–0.01 wt.%), which means that the isotope ratios recorded in these calcites would be sensitive to small perturbations in fluid isotopic composition. In comparison, calcites formed in equilibrium with the normal Sr content of seawater should have about 0.1 wt.% Sr or greater (see Bathhurst, 1975, p. 262 for summary). This indicates that the fault calcite has probably not precipitated from unmodified seawater. The relatively radiogenic values probably indicate addition of radiogenic ^{87}Sr from detrital potassium-bearing phases by the ascending hot fluids or by descending meteoric water.

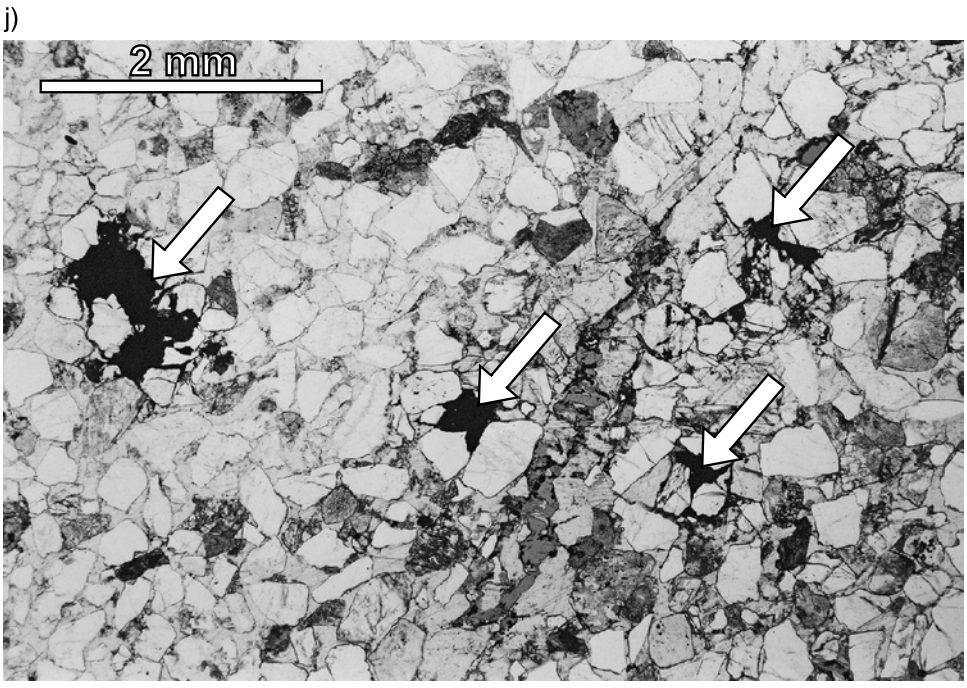

Figure 3. Continued. (j) Hematite cement (arrows) in sandstone adjacent to Refugio-Carneros fault zone. Sample from location A, Figure 1b. Plain light.

Trace-Element Content of Calcite (Mn, Mg, Fe)

The trace-element composition of carbonate minerals gives clues as to the type of fluids present at the time of crystallization. As reviewed by Boles (1998) and also shown in Morad (1998), marine calcite is commonly Mg enriched, whereas calcite forming in meteoric water along basin margins has relatively low trace-element contents and proportionally high Mn contents relative to Mg and Fe.

Microprobe analyses of seven vein samples for Mg, Mn, and Fe show that the fault calcite is generally relatively pure, with the total of Mg + Fe + Mn being less than about 2 mol% (Table 4; Figure 6). The proportions of Mg, Fe, and Mn differ between samples from the east and west parts of the Refugio-Carneros fault. Western samples are relatively rich in Mn, whereas eastern samples have more Mg. Fe is relatively low in both suites.

Magnesium-rich calcites are commonly formed during early diagenesis of marine sandstones as a result of the initial relatively high Mg content of trapped seawater. Magnesium contents of 5–10% are common (see, e.g., Boles et al., 1985). The fault calcites are relatively low in Mg, which is consistent with crystallization from relatively Mg-depleted marine basin water. Such waters are found in petroleum basins of southern California at temperatures in excess of 100°C (e.g., see Fisher and Boles, 1990) Thus, the water in the fault zone is consistent with diagenetically evolved seawater, instead of unmodified seawater. The elevated temperatures at which these calcites appear to have formed should cause increased trace-element substitution (e.g., Boles, 1998). High-temperature crystallization of calcite from Mg-rich seawater should result in Mg-rich calcite, as increased Mg substitution is favored at higher temperature. Thus, the relatively low Mg content of these calcites infers that the fault water

Table 2. Fluid-Inclusion Data from Calcite Cements in Refugio-Carneros Fault Zone*

Sample	Mean T_h (aq)	*n*	Salinity (wt.%)	*n*	Mean T_h (hc)	*n*	Data Source
RF 1A-4	104 ± 9	16	0.35% ± 0.02	10	not determined		data from Fluid Inc.
RF 2A	91 ± 15	24	3.25% ± 5.9	11	89 ± 6	5	data from Fluid Inc.
MAT-1	83 ± 3	10	1.4% ± 0.5	9	not recorded		data from Renee Perez

*See Table 3 for location of samples. T_h (aq) is aqueous fluid homogenization temperature in °C. T_h (hc) is hydrocarbon homogenization temperature in °C. Salinity (wt.%) is fluid salinity as weight % NaCl estimated from freezing temperature. *n* = number of measurements.

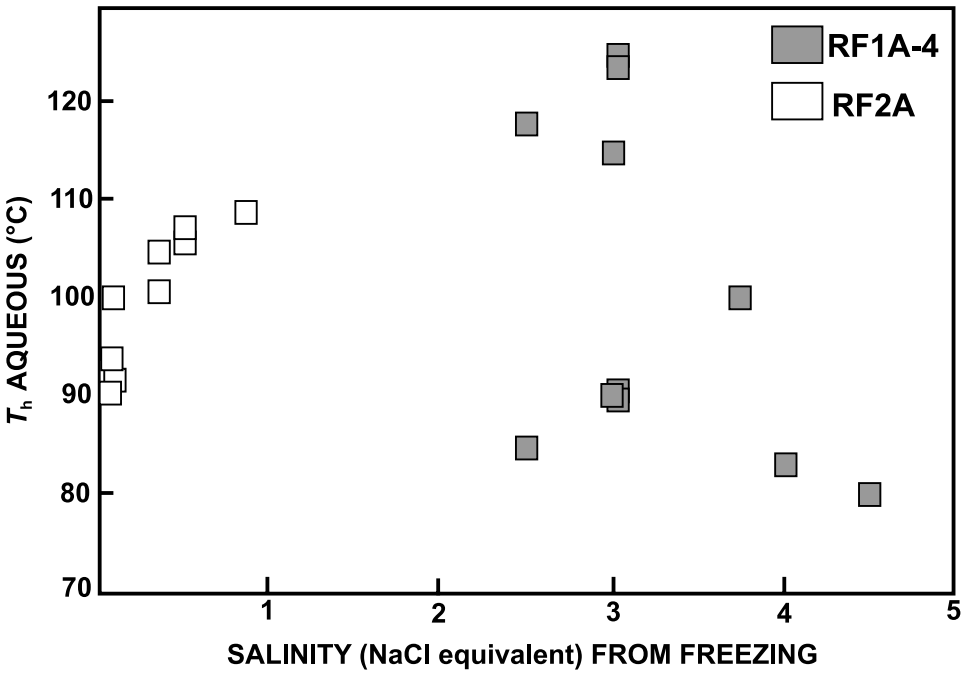

Figure 4. Homogenization temperatures (T_h) plotted against salinity estimates for fluid inclusions from Refugio-Carneros fault calcites. Salinity is in weight percent NaCl equivalent. Data from Table 2.

was Mg-depleted water, consistent with diagenetically evolved marine formation water derived from the subsurface (Table 1). The relative Mn-rich trace-element content of some samples might indicate a meteoric influence. Manganese-enriched calcites are common in the San Joaquin marine basin margins because of meteoric incursions (Hayes and Boles, 1993; Lee and Boles, 1996).

Overall, the trace-element content of these calcites is relatively low compared with calcite cements in sandstones that have formed at comparable temperatures during burial diagenesis (e.g., Boles and Ramseyer, 1987; Boles, 1998). The difference is believed to be caused by the dilution of the deep-basin brine by shallow meteoric water.

BASIN-MARGIN PALEOHYDROLOGY

Water and Gas Source

Present-day offshore waters from Monterey producers in the Santa Barbara area have oxygen isotopic compositions ranging from +1 to +6‰ (table 5 in Eichhubl and Boles, 1998; Table 1, this paper). Present-day meteoric-derived shallow groundwater in the Santa Barbara area is about $\delta^{18}O_{SMOW}$ −7 to −8‰ (SMOW = standard mean ocean water) (Rademacher et al., 2003). Fluid inclusions suggest crystallization temperatures of 80–120°C. Using isotope fractionation factors of Friedman and O'Neil (1977) and calcite oxygen isotopes values of −9.5 to −11‰, isotopic composition of the water in the fault zone would be about 0 to +4‰. This indicates that fault water was dominantly seawater or slightly evolved marine water from the subsurface instead of meteoric water. The present-day geothermal gradient in the Santa Barbara basin is about 50°C/km (81°C/mi) based on shut-in well temperatures at Platform Holly of about 58°C at a depth of 1060 m (3480 ft). Calcite crystallization temperatures of about 80–120°C would require fluids to come from a minimum depth of at least 1.5 km (1 mi). This is a minimum depth because some heat loss would occur during transport toward the surface. The Santa Barbara coastal area in the vicinity of the Refugio-Carneros fault has no known volcanic or local intrusive activity that could account for elevated temperatures at a near-surface to surface outcropping fault after the Miocene. Therefore, hot, basinal fluids must have been driven up the fault zone from depth in the adjacent sedimentary basin to the south.

Oxygen isotopic values of the calcite are relatively uniform, differing by only a few per mil, which indicates that the crystallization conditions (i.e., temperature and isotopic composition of the fluid) in the fault zone were relatively uniform. To maintain relatively constant temperature and isotopic composition of a

Table 3. Calcite Oxygen-Carbon Isotopic Analyses from Refugio-Carneros Fault Zone and Associated Sandstone*

Analyses	Sample	Crystal Type	Distance from Main Fault (m)	Oxygen PDB	Carbon PDB	Comments
West End of Fault–Vein Calcite						
Westernmost end of fault as mapped by Dibblee (1988), gully west side of Figure 1b						
1	RF-16	blocky	0	−10.885	−35.928	crystals in fault wedge
Float on hillslope above locality A of Figure 1b						
2	RF-10A	blocky	<2	−10.832	−35.617	crystals 5–20 mm (0.2–0.8 in.) mixed with breccia crystals 2–3 mm (0.08–0.12 in.), float
3	RF-10B	blocky	<2	−10.832	−38.472	crystals 1–2 mm (0.04–0.08 in.), brecciated, float
Locality A of Figure 1b						
4	RF-11A	blocky	0	−11.297	−23.052	crystals to 3 mm (0.12 in.), massive, 30 cm (12 in.) from hanging wall
5	RF-11B	blocky	0	−11.226	−26.448	crystals 1–2 mm (0.04–0.08 in.), shear zone, 30 cm (12 in.) from hanging wall
6	RF-12	blocky	0	−10.665	−39.618	crystals 2–4 mm (0.08–0.16 in.), brecciated zone on footwall of fault
7	RF-13	blocky	0	−10.828	−34.357	crystal 70 × 70 mm (2.7 × 2.7 in.), single crystal, 50 cm (20 ft) above footwall
8	RF-14	blocky	0	−10.544	−38.619	crystals 3–8 mm (0.12–0.31 ft), massive, next to hanging wall
9	RF-15	blocky	0	−11.113	−41.278	crystals 3–7 mm (0.12–0.28 in.) in 3–10-mm (0.12–0.4 in.) veins within oxidized sandstone
North to south traverse across 1-m (3.3-ft)-thick fault cement at locality B of Figure 1b						
10	RF3A-1	blocky	0	−10.306	−39.088	hanging wall, north side
11	RF3B-1	blocky	0	−8.481	−23.698	sample 0.25 m (0.82 ft) from north side
12	RF3C-1	blocky	0	−10.365	−23.240	sample 0.75 m (2.45 ft) from north side
13	RF3D-1	blocky	0	−10.425	−40.836	footwall, south side
Locality E of Figure 1b						
Veins 0.5–1 cm (0.2–0.4 in) thick in sandstone						
14	RF2C-1	blocky	1	−10.438	−34.885	youngest vein
15	RF2C-2	blocky	1	−10.018	−37.008	oldest vein
1 km (0.62 mi) east of eastern edge of Figure 1b locality						
Banded calcite with crosscutting veins (sample with evidence for episodic fluid flow)						
16	RF1A-A	blocky	<1	−10.275	−29.170	5 mm (0.2 in.) vein on outer edge of rock
17	RF1A-B	blocky	<1	−9.948	−28.865	centimeter-thick vein cutting sandstone matrix

18	RF1A-D	blocky	<1	−10.449	−31.939	1 cm (0.4 in.) vein which cuts all layers
19	RF1A-C	acicular	<1	−10.249	−30.772	acicular crystals, 1–10 mm (0.04–0.4 in.), in bands
20	RF1A-3a	acicular	<1	−10.381	−30.763	acicular crystals, 1–10 mm (0.04–0.4 in.), in bands
21	RF1A-3b	acicular	<1	−10.543	−29.514	acicular crystals, 1–10 mm (0.04–0.4 in.), in bands
22	RF1A-4a	acicular	<1	−10.294	−30.368	acicular crystals, 1–10 mm (0.04–0.4 in.), in bands
23	RF1A-4b	acicular	<1	−10.415	−30.233	acicular crystals, 1–10 mm (0.04–0.4 in.), in bands
24	RF1A-5a	acicular	<1	−10.495	−30.357	acicular crystals, 1–10 mm (0.04–0.4 in.), in bands
25	RF1A-5b	acicular		−10.445	−30.270	acicular crystals, 1–10 mm (0.04–0.4 in.), in bands
Large single crystal						
26	RF1B-1	blocky	0	−11.067	−41.300	single calcite crystal, 2.5 cm (1 in.)
27	RF1B-2	blocky	0	−11.354	−41.635	single calcite crystal, 2.5 cm (1 in.)
West End of Fault, Sandstone Matrix						
Locality E of Figure 1b				B		
28	RF2C-1a		1	−10.461	−29.236	sandstone matrix
29	RF2C-1b		1	−10.462	−28.459	sampled 2 mm (0.08 in.) from RF2C-1a
30	RF2C-2		1	−8.098	−23.075	sampled 2 cm (0.8 in.) of RF2C-1a
1 km (0.62 mi) east of eastern edge of Figure 1b locality						
31	RF1A-1a		<1	−10.023	−26.776	sandstone matrix
32	RF1A-1b		<1	−10.016	−26.569	sampled 2 mm (0.08 in.) from RF1A-1a
33	RF1A-2		<1	−7.887	−10.700	Sampled 15 cm (6 in.) from RF1A-1a
East End of Fault						
Outcrop in small road cut 15 m (49 ft) west of ravine locality, Goleta, California						
Main fault cement						
34	JM-1A	blocky	0	−10.710	−39.324	crystals 20–40 mm (0.8–1.6 in.)
35	JM-1B	blocky	0	−10.801	−35.779	crystals 2–3 mm (0.08–0.12 in.), shear zone
Ravine locality						
Veins 0.5–2 cm (0.2–0.8 in.) thick in sandstone						
36	MAT2-A1	blocky	2	−10.122	−34.920	crystals 5 mm (0.2 in.)
37	MAT2-A2	blocky	2	−10.082	−34.084	crystals 5 mm (0.2 in.)
38	MAT2-A3	blocky	2	−10.149	−33.963	crystals 5 mm (0.2 in.)
39	MAT2-B1	blocky	2	−9.500	−34.237	crystals 5 mm (0.2 in.)
40	MAT2-B2	blocky	2	−10.199	−33.998	crystals 5 mm (0.2 in.)
41	MAT2-B4	blocky	2	−10.434	−34.016	crystals 5 mm (0.2 in.)

Table 3. Continued

Analyses	Sample	Crystal Type	Distance from Main Fault (m)	Oxygen PDB	Carbon PDB	Comments
42	MAT2-C1	blocky	2	−10.216	−34.761	crystals 5 mm (0.2 in.)
43	MAT2-C2	blocky	2	−10.257	−33.585	crystals 5 mm (0.2 in.)
44	MAT2-D1	blocky	2	−10.156	−34.796	crystals 5 mm (0.2 in.)
45	MAT2-D2	blocky	2	−10.400	−34.876	crystals 5 mm (0.2 in.)
46	MAT2-E1	blocky	2	−10.494	−32.364	crystals 5 mm (0.2 in.)
Large, 50–70-mm (2–2.8-in.) acicular crystal sprays of calcite						
Traverse along length of individual crystals from base to top						
47	MAT3-A1	acicular	2.5	−9.954	−39.972	traverse A, base
48	MAT3-A3	acicular	2.5	−10.173	−38.298	traverse A
49	MAT3-A4	acicular	2.5	−10.144	−38.704	traverse A
50	MAT3-A5	acicular	2.5	−10.237	−38.904	traverse A
51	MAT3-A6	acicular	2.5	−10.272	−38.728	traverse A
52	MAT3-A7	acicular	2.5	−10.120	−38.212	traverse A, top
53	MAT3-B1	acicular	2.5	−10.093	−37.637	traverse B, base
54	MAT3-B2	acicular	2.5	−10.036	−38.456	traverse B
55	MAT3-B3	acicular	2.5	−10.176	−38.149	traverse B, top
56	MAT3-C1	acicular	2.5	−9.964	−37.737	traverse C, base
57	MAT3-C2	acicular	2.5	−9.858	−37.825	traverse C
58	MAT3-C3	acicular	2.5	−10.342	−39.146	traverse C
59	MAT3-C4	acicular	2.5	−10.006	−37.914	traverse C, top
60	MAT3-D1	acicular	2.5	−10.272	−37.541	traverse D, base
61	MAT3-D2	acicular	2.5	−10.455	−38.314	traverse D, top
62	MAT3-E1	acicular	2.5	−10.494	−32.364	traverse E, base
63	MAT3-E4	acicular	2.5	−10.383	−39.071	traverse E
64	MAT3-E5	acicular	2.5	−10.165	−38.523	traverse E
65	MAT3-E6	acicular	2.5	−8.949	−38.260	traverse E, top
66	MAT3-F1	acicular	2.5	−10.456	−39.104	traverse F, base
67	MAT3-F2	acicular	2.5	−10.281	−38.938	traverse F
68	MAT3-F3	acicular	2.5	−10.071	−38.238	traverse F
69	MAT3-F4	acicular	2.5	−10.246	−40.115	traverse F, top
70	MAT3-G1	acicular	2.5	−9.662	−36.976	traverse G, base

71	MAT3-G2	acicular	2.5	−10.018	−38.663	traverse G
72	MAT3-G3	acicular	2.5	−9.734	−37.907	traverse G, top
73	MAT3-H1	acicular	2.5	−9.602	−38.191	traverse H, base
74	MAT3-H2	acicular	2.5	−10.042	−38.363	traverse H, top
75	12A	acicular	1.5	−10.048	−37.236	spot sample
76	13A	acicular	1.5	−10.293	−36.017	spot sample
Blocky crystals recrystallized from acicular sprays						
77	12B	blocky	1.5	−10.768	−39.539	

*Isotopic analyses from J. Kennett Lab, University of California, Santa Barbara, and L. Stott Lab, University of Southern California, California.

fluid, flow volumes must be relatively large and sourced from a uniform reservoir. Considering that the oxygen isotopic range of natural waters could range as much as 15 ‰ (i.e., varying from evolved connate waters of +5 ‰ to isotopically light meteoric waters of −10 ‰), it is clear that the fluids were relatively well mixed and were of uniform composition. The volume of crystallized calcite also suggests that fluid volumes passing through the fault zone were relatively high.

The oxidation of methane requires an oxidizing fluid. Deep subsurface waters are in a reduced state and are low in sulfate ion because of the reducing properties of hydrocarbons and hence would not be a potential oxygen source (see Table 1). Anaerobic oxidation from unaltered seawater is a possibility because of the relatively high content of sulfate ion (Table 1), which is a potential oxidant (e.g., Machel et al., 1995). However, reduction of sulfate ion would release sulfide, and evidence is lacking for Fe sulfide precipitates (e.g., pyrite). This suggests that seawater sulfate was not the source of oxygen, and that the calcite was not coming in direct contact with unaltered seawater. The occurrence of hematite (Figure 3j) suggests highly oxidizing conditions. The most likely source of oxygen was dissolved oxygen in meteoric water. Modern groundwaters in the Vaqueros sandstone at the eastern end of the fault (60–150 m [−490 ft] deep) are relatively high in sulfate (Table 1) and sometimes in nitrate, suggesting relatively oxidizing conditions in these waters. The low salinity value of some fluid inclusions (Table 2) confirms the presence of meteoric water.

The extremely light carbon isotopic composition of many of the calcites ($\delta^{13}C_{PDB}$ −30 to −40 ‰) indicates oxidation of methane (e.g., Hathaway and Degens, 1969; Donovan et al., 1974; Whiticar and Faber, 1986). Methane presently found in offshore reservoir gas at Platform Holly and nearby seeps has an isotopic composition of about −40 to −45 ‰ (J. R. Boles, unpublished data).

Gas fields that may have leaked methane are located downdip of the western and eastern parts of the Refugio-Carneros fault, including the Refugio Cove gas field and the Capitan oil field in the western part, and the La Goleta gas field in the eastern part of the fault (Figure 1a). More likely, because of the association with relatively high-temperature fluids, the methane may have been derived directly from the source rocks in the basin having bypassed hydrocarbon reservoirs. It seems unlikely that fluids have come from the Santa Ynez fault (Figure 1a) or areas north of this fault because of the lack of hydrocarbons in that region.

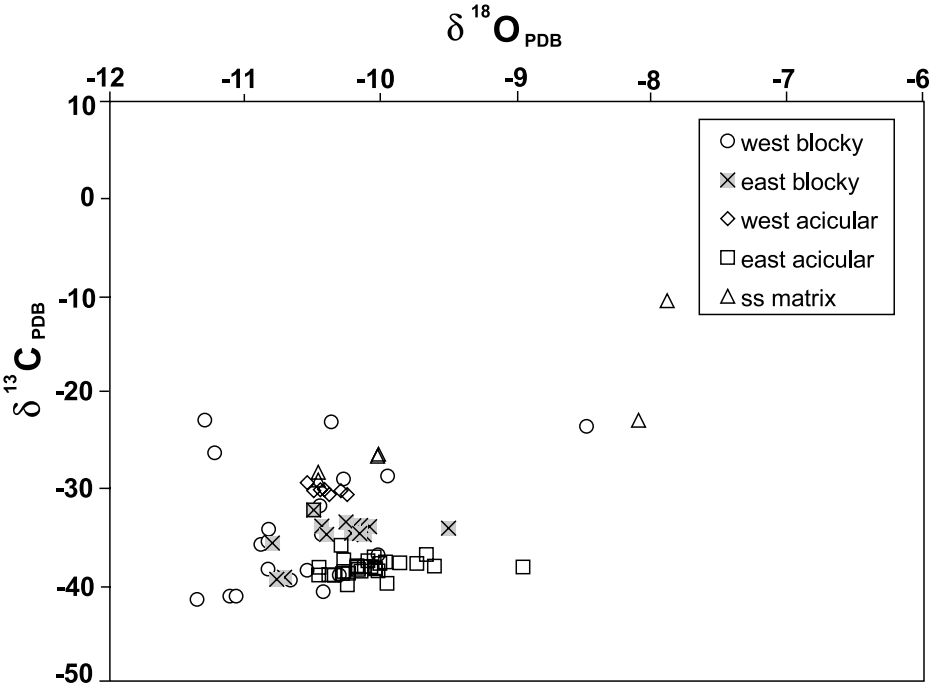

Figure 5. Oxygen and carbon isotopic values from calcite associated with the Refugio-Carneros fault. Data from Table 3. Units are per mil.

Mass Balance Constraints for Methane and Water

The amount of gas required to account for the observed mass of calcite is relatively small. Assuming a generalized methane oxidation reaction of

$$CH_4 + 2O_2 = CO_2 + 2H_2O$$

1 mol of calcite (37 cm^3; 2.3 $in.^3$) requires a minimum of 1 mol of CO_2 by a reaction of

$$H_2O + CO_2 + Ca^{2+} = CaCO_3 + 2H^+$$

For example, for the 338-m^3 (11,900-ft^3) mass of calcite at that western part of the fault (Figure 1b, location A), this amounts to about 10^8 L of CO_2 (at 25°C, 1 atm). This amount of gas is less than 1% of the produced gas for the nearby Refugio Cove gas field, which is 2.7 km (1.7 mi) downdip. Thus, a small volume of methane leakage can produce relatively large calcite accumulations.

The volume of aqueous solution required to precipitate these calcite deposits, however, is comparably large because of the low solubility of calcite in water. For an observed mass of calcite of $10^{6.7}$ mol (338 m^3;

Table 4. Microprobe Data of Fault Calcite*

		Mg		Mn		Fe	
Sample	Number of Spots	Average	Standard Deviation	Average	Standard Deviation	Average	Standard Deviation
MAT-2 vein traverse	49	0.499	0.220	0.666	0.132	0.030	0.040
MAT-2 sandstone matrix	3	0.735	0.293	0.963	0.289	0.012	0.021
MAT-3 vein traverse	23	0.680	0.205	0.768	0.085	0.036	0.040
RF-11 vein traverse	93	0.047	0.056	0.451	0.092	0.043	0.039
RF-11 area A	6	0.056	0.063	0.406	0.121	0.066	0.056
RF-11 area B	11	0.072	0.112	0.482	0.110	0.036	0.039

*In mol%. Normalized with calcium to 100 mol%. Sr and Ba each present at less than 0.02 wt.%, most less than 0.01 wt.%. See Table 3 for location of samples.

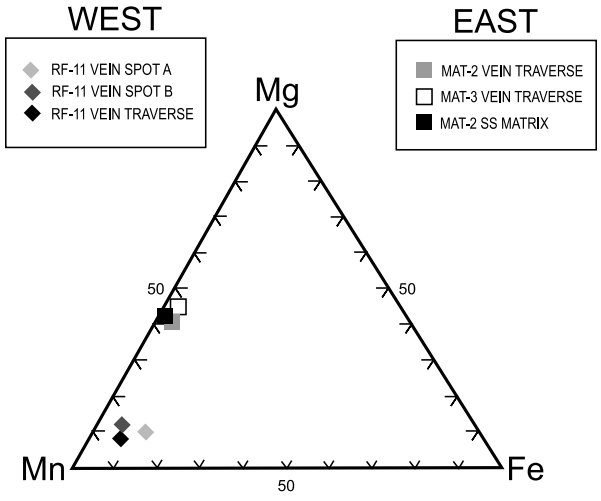

Figure 6. Ternary plot of Mn, Mg, and Fe in fault calcite. Data from Table 4.

11,900 ft^3), activities of Ca^{2+} and CO_3^{2-} assumed to be roughly equal, and for a solubility product of calcite at 80°C of $[Ca^{+2}][CO_3^{-2}] = 10^{-8.6}$, then less than $10^{-4.6}$ mol of calcite would be precipitated from each liter of fluid passing through the fault zone. Thus, a minimum of $10^{11.2}$ L or 1.6×10^8 m^3 (5.6×10^9 ft^3) of fluid would be required to produce the volume of observed calcite. Assuming the porosity in the Vaqueros sandstone is 20%, and the formation is 112 m (367 ft) thick, this is equivalent to draining the fluid from a cylinder of the sandstone with an approximate radius of 1.5 km (1 mi). This estimate is comparable to a radius of influence of 4–12 km (2.5–7 mi) obtained by Eichhubl and Boles (2000a) for a fault hosted in siliceous mudstone of the Miocene Monterey Formation at the western end of the Santa Ynez fault system. Whereas their estimate was derived for a fault hosted in a different rock type, both fault locations are in a similar structural setting along the northern flanks of the Santa Barbara basin.

Finite-Element Modeling of Fluid Flow and Heat Transfer

To quantify fault-controlled fluid and heat transport, we have developed finite-element simulations for both steady flow and transient flow in the coastal Santa Barbara cross section shown in Figure 2. Fluid and heat transport in faulted, saturated strata can be mathematically modeled by solving continuum-based flow equations representing conservation of fluid mass, flow vorticity, and thermal energy. Numerical solutions to the flow equations are required for the model to accommodate the nonlinearity in fluid properties, effects of convective flow on heat transport, and multidimensional effects on flow because of heterogeneity in permeability and thermal conductivity.

The first step in our hydrogeologic modeling is to solve for the Darcy flow field for variable-density flow using the theory, model parameters, and finite-element code JHU2D/CPFLOW (Johns Hopkins University/coupled flow model) as described in Raffensperger (1996). The result is a coupled mathematical model for steady-state and/or transient fluid flow and heat transport in a nondeforming, two-dimensional profile. Fluid density and viscosity are assumed to depend on pressure, temperature, and salinity according to the equations of state for NaCl-type fluids programmed in Raffensperger and Garven (1995). For the applications discussed later, we assume a uniform salinity everywhere in the flow field and focus on the nature of fluid and heat flow in a coastal sedimentary profile with normal faults. Issues of fluid mixing and the transient evolution of fluid composition, mineralization, and geochemical reactions require development of transient solute-transport calculations with RST2D (reactive solute transport, two-dimensional), such as the type described in Appold and Garven (1999, 2000) and Wilson et al. (1999), and these effects will be discussed in a later publication.

For finite-element modeling of the paleohydrology, the geologic profile has been restored to approximately 100 ka, when sea level had submerged much of the stratigraphic profile except for the more elevated Santa Ynez terrane north of the fault. The Vaqueros sandstone is assumed to be the principal sandstone aquifer in the modeled north-south profile. The model domain is more than 3 km (1.9 mi) thick and extends laterally for 13 km (8 mi) (Figure 7). The Vaqueros sandstone is buried by more than 300 m (1000 ft) of Miocene mudstone of the Rincon and Monterey formations near the Refugio-Carneros fault, and this section thickens offshore because of rapid Pliocene and Pleistocene sedimentation in the basin. Older and less permeable Tertiary mudstone, siltstone, and sandstone underlie the Vaqueros, and these formations crop out in the Santa Ynez Mountains. In addition to the Refugio-Carneros fault, the model included the subparallel Coast fault, which is located 4 km (2.5 mi) south of the Refugio-Carneros fault.

Nine hydrogeologic units have been discretized using a finite-element mesh comprised of 2925 quadrilateral-shaped elements (45 rows and 65 columns); the mesh is finer in both the Refugio-Carneros and Coast faults to capture detail in these 100-m (330-ft)-wide

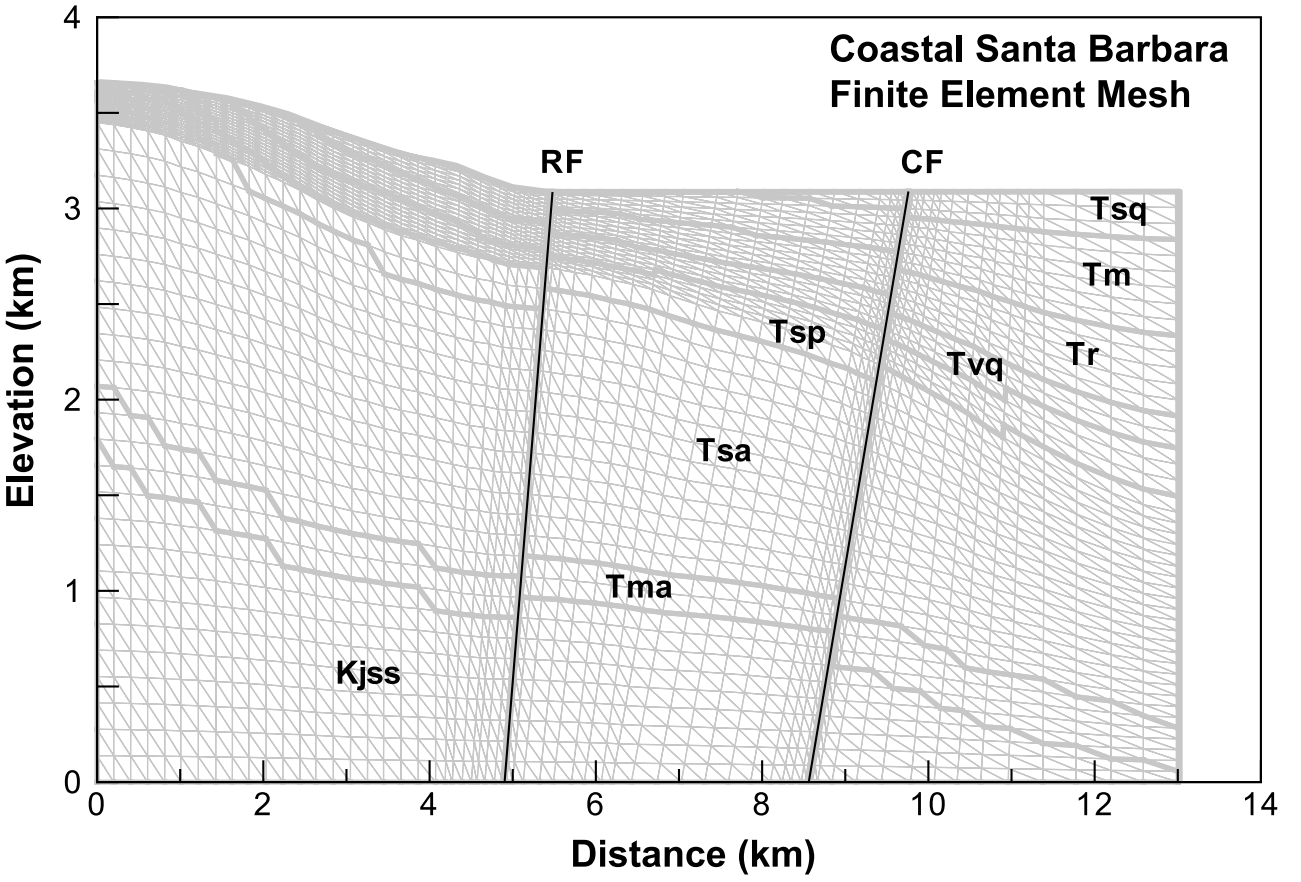

Figure 7. Coastal Santa Barbara finite-element mesh used in fluid-flow calculations. Mesh based on cross section shown in Figure 2. RF = Refugio-Carneros fault, CF = Coast fault, Tsa = Alegria, Gaviota, and Sacate formations, Tma = Matilija Sandstone, Kjss = Jalama Formation. See key in Figure 2 for other strata.

damage zones. Model parameters were chosen to be representative of formation properties (permeability, porosity, thermal conductivity, etc.) known from present-day petroleum reservoirs. The Vaqueros aquifer is assigned a porosity $n = 20\%$, a lateral permeability $k_x = 10^{-13}$ m^2 (100 md), and vertical permeability $k_z = 10^{-15}$ m^2 (1 md). Other hydrostratigraphic formations in the profile are assigned anisotropic permeabilities from 1 to 1000 times lower, except for the Refugio-Carneros fault, which is assigned an isotropic permeability of $k_x = k_z = 10^{-13}$ m^2. The section is submerged by a few hundreds of meters of seawater south of the Refugio fault, but north of the coast, it becomes subaerial such that a meteoric water table is assigned atmospheric pressure to the top row of mesh nodes. Both the left (north) and right (south) sides of the finite-element mesh serve as hydrologic divides (no lateral flow boundary). A constant heat flow of 90 mW/m^2 is assigned to the base of the mesh and represents elevated crustal heat flow along the continental margin.

Simulations were first conducted to test the thermal effects of steady-state groundwater flow caused by simple topographic relief along the coastal ranges of the Santa Ynez Mountains. In this scenario, meteoric groundwater from the elevated terrane is driven seaward from the outcrop areas, and fluid flow is focused laterally by the high-permeability Vaqueros Formation. Meteoric groundwater is driven offshore as far as a few kilometers, with most seepage focused to the seafloor along the Refugio-Carneros and coast faults, which channel vertical discharge and thus prevent cross-fault flow. Offshore seepage rates are predicted to be relatively small because of the weak driving force. These upward flow rates are too slow to move hot water to the surface under this hydrologic scenario.

A second set of modeling experiments were conducted to test the effects of transient flow caused by fault venting. In this scenario, we assume that the submarine part of the finite-element mesh has been overpressured to about 80% of lithostatic pressure because

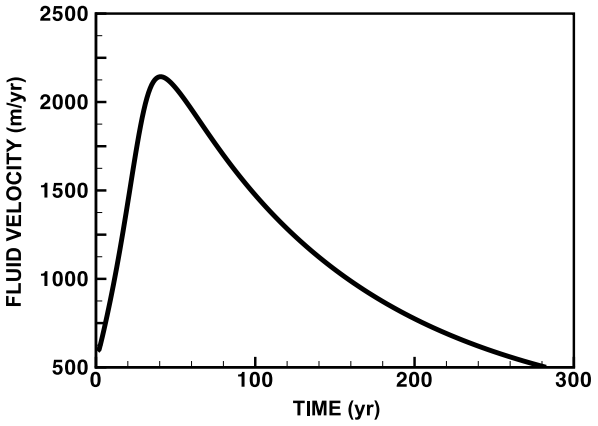

Figure 8. Calculated fluid velocities at 300-m (1000-ft) depth in the Refugio-Carneros fault during venting. See text for calculations.

of tectonic forces squeezing the sedimentary wedge offshore and because of petroleum generation as the sediments are deeply buried. To begin the hydrogeologic simulation, the overpressured section is allowed to vent, assuming the Refugio-Carneros fault is activated as a flow conduit first, and we then track the transient pressure and temperature field through time, until the excess pressures have dissipated. The model parameters are the same as described previously. Results show that the overpressured fluids regionally drain through the sand aquifer and vent rapidly along the Refugio-Carneros fault. Flow rates in the fault zone near the top of Vaqueros sandstone are predicted to peak at about 2000 m/yr (6600 ft/yr), about 50 yr after rupture, but this rate decays exponentially over a few hundred years (Figure 8). Heat transport is a much slower process, and therefore, the thermal decay history is much longer. The transient-flow model predicts a burst of cold formation water right after fault rupture, followed by a stream of hotter water, where the temperature peaks at 110–120°C. Temperature gradually falls below 100°C about 1000 yr after rupture (Figure 9).

The transient flow rates predicted above likely represent an extreme estimate, as the model does not take into account the small scale and structural complexity of faulted sandstones (Antonellini and Aydin, 1994; Davatzes et al., 2003), the effects of diagenetic-hydrothermal reactions during flow, the effects of hydrologic feedback on deformation, or the effects of sea level and salinity changes over time. However, these first-order estimates are probably realistic and suggestive of the timescales and types of processes affecting structurally controlled fluid migration in the Refugio-Carneros fault area.

Effect of Sea Level Changes on Meteoric Recharge

The presence of meteoric water in the Refugio-Carneros fault indicates that the southward tilting of the Santa Ynez Mountains was sufficient to subaerially expose the rocks and allow meteoric recharge into south-dipping permeable layers and/or directly into the fault zone from above. This means that at least during some periods, perhaps accelerated during the four sea level lowstands of the 100,000–500,000-yr period (Rohling et al., 1998), meteoric incursions were significant. Present-day formation waters from offshore hydrocarbon-producing fields are progressively more saline in an offshore direction, showing that mixing of meteoric water with the original marine water has occurred (Table 1).

The current tectonic uplift rate along the Santa Barbara coast exceeds recent sea level rise by 1–2 mm/yr (0.04–0.08 in./yr) based on dating of marine terraces that are less than 100,000 yr old (Gurrola et al., 2001). Extrapolating this uplift rate for the 110,000–500,000-yr age of cementation, the area would be about 110–1000 m (360–3300 ft) lower in elevation than it is today. The present position of the calcite-cemented fault is from 120 to 180 m (390 to 590 ft) above sea level. Thus, because past sea level was as much as 120 m (390 ft) below present levels (Rohling et al., 1998), it is likely that the coastal area near the western end of the fault, at least, was below sea level for most of the calcite cementation, assuming current coastal uplift rates. Uplift rates would have to be an order of magnitude lower than current estimates to

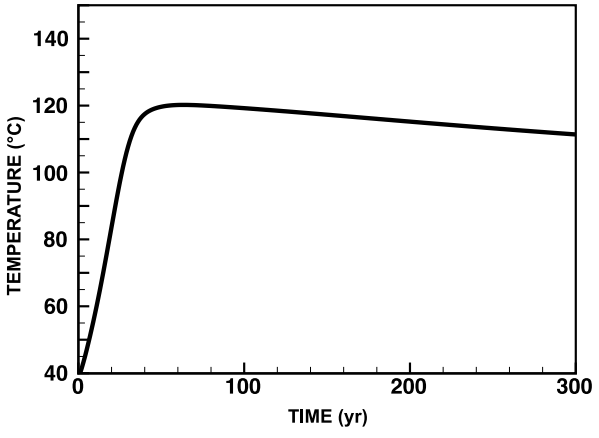

Figure 9. Calculated fluid temperatures at 300-m (1000-ft) depth in the Refugio-Carneros fault during venting. See text for calculations.

place the western outcrops above sea level. Further north, the crest of the Santa Ynez Mountains was apparently exposed to influx of meteoric water.

Comparison to Observations in the Coastal Monterey Formation

The evidence shown here supports the conclusions of many previous workers that fluid movement is actively associated with fault rupturing (e.g., Sibson, 1994; Eichhubl and Boles, 2000b). Episodic fluid pulses transporting mineral grains are similar to those described by Eichhubl and Boles (2000b) for carbonate breccia fragments (>2 cm [>0.8 in.] in size) in the Jalama Beach fault near Point Conception in the Monterey Formation.

Winter and Knauth (1992), Eichhubl and Boles (1998, 2000a, b), and Martin and Rymerson (2002) have described a series of fault-related carbonates in the coastal Monterey Formation from Jalama Beach, near Point Conception, at Arroyo Burro Beach near Santa Barbara and some smaller scale vein systems (Figure 1a). These occurrences are similar to the Refugio-Carneros fault system in terms of showing repeated episodes of fluid movement and cementation and having relatively high temperature based on fluid inclusions (Bodnar, 1990; Eichhubl and Boles, 2000b). They also are associated hydrocarbons, which largely postdate the carbonate emplacement in these faults. They mainly differ in mineralogical composition (the Jalama Beach occurrence is dolomite and late-stage quartz), and in contrast to the extremely light carbon isotopic signature in the Refugio-Carneros calcite, they exhibit relatively heavy carbon isotopes. At Jalama Beach, the dolomites have carbon values between -5 and -20‰, with the mean being about -15‰. At Arroyo Burro and its vicinity, the calcite is extremely heavy, with carbon isotopic values ranging from 0 to +16‰. Apparently, methane oxidation was much more common in the Refugio-Carneros fault than in these other examples, perhaps because of its close proximity to an oxygenated meteoric source.

Comparison of Modern and Ancient Seeps in the Coastal Area

There are significant differences between the hydrocarbon seeps in the Refugio-Carneros fault system and the modern offshore seeps in the Santa Barbara Channel. The ancient seeps were hot and must have involved substantial flux of very hot water up the fault. The offshore Ellwood fault (Figure 1a) is presently the site of natural leakage of methane (Hornafius et al., 1999; Eichhubl et al., 2000; Boles et al., 2001).

Fluid pressures, at the time of development in the 1960s, at Platform Holly in the Monterey reservoir were approximately 10% over hydrostatic pressure at about 1-km (0.62-mi) subsea depth. At Platform Hondo, initial pressure in the Monterey Formation at 2.6 km (1.6 mi) subsea was 15% less than hydrostatic, whereas pressures at 3-km (1.9-mi) depth in the underlying Vaqueros sandstone were about 15% over hydrostatic pressure (data from Mineral Management Service, U.S. Department of Interior). Thus, we would not expect hot fluids to be coming from these depths because of lack of a pressure gradient. Our modeling demonstrates that the offshore section was likely highly overpressured several hundred thousand years ago and has since dissipated the pressure, possibly because of basin deformation.

Modern gas seeps in the vicinity of Platform Holly, captured by giant seafloor tents (Boles et al., 2001), do not appear to be associated with hot water. In addition, remote-operated vessel surveys from the 1980s, which were conducted prior to emplacement of the collection tents, did not report any carbonate accumulations. More recent detailed remote-operated vessel studies by Monterey Bay Aquarium Research Institute in the Santa Barbara Channel (Eichhubl et al., 2000) also indicate the modern gas seeps do not involve detectable quantities of deep formation water coming to the surface. Carbonate nodules and crusts are common in the sediment and on the seafloor in the area, and these are reported to be made of aragonite, high-Mg calcite, and dolomite (Eichhubl et al., 2000), which are different from the Refugio-Carneros fault calcite. To date, there have been no reports of carbonate in the offshore area like that in the Refugio-Carneros fault zone.

CONCLUSIONS

Field, petrologic, and geochemical studies show that calcite in the Refugio-Carneros fault zone has been derived from the oxidation of methane during episodic fluid expulsions related to faulting. Fluid inclusions show that hydrocarbons were present with hot fluids, indicating that the fluids were derived from depth in the Santa Barbara basin. Salinities are variable, indicating the presence and mixing of both dilute and saline water. Geochemical conditions in the fault were highly oxidizing, presumably from mixing of shallow oxygenated groundwater with the basinal fluids.

As shown in our fluid-flow modeling, the offshore area is a likely source of saline fluid and hydrocarbons, which we calculate to be expelled from overpressured strata in the Monterey Formation. At the time the fault was active, we infer the fault was plumbed into the offshore basin, where Monterey and older formations contain diagenetically modified seawater with salinities of around 3.5 wt.%. The uplift of the Santa Ynez Mountains north of the fault has created a hydraulic head to drive fresh oxygenated water down permeable sandstone beds into the fault. Thus, the fault appears to have been a mixing zone between meteoric water derived from the north and upward-moving hot formation water and hydrocarbons rising from the deep basin to the south.

The overall picture indicates an evolution in fluid pressure over a period of several hundred thousand years. Initially, during the period from at least 500 ka to as recent as 100 ka, overpressured hot formation water and hydrocarbons rapidly migrated up to the basin flanks from kilometers depth in the Earth's crust and was released along the lateral parts of a coastal fault. Continued deformation in the basin ultimately resulted in the release of the overpressured fluids. At present, fluid pressures are close to a hydrostatic condition (at the time of offshore oil development) resulting in passive, buoyancy-driven seepage of hydrocarbons without substantial formation water.

REFERENCES CITED

Antonellini, M., and A. Aydin, 1994, Effects of faulting on fluid flow in porous sandstones: Petrophysical properties: AAPG Bulletin, v. 78, p. 355–377.

Appold, M. S., and G. Garven, 1999, The hydrology of ore formation in the southeast Missouri district: Numerical models of topography-driven fluid flow during the Ouachita orogeny: Economic Geology, v. 94, p. 913–935.

Appold, M. S., and G. Garven, 2000, Reactive flow models of ore formation in the southeast Missouri district: Economic Geology, v. 95, p. 1605–1626.

Atwater, T., 1970, Implications of plate tectonics for the Cenozoic tectonic evolution of western North America: Geological Society of America Bulletin, v. 81, p. 3513–3535.

Aydin, A., 2000, Fractures, faults, and hydrocarbon entrapment, migration and flow: Marine and Petroleum Geology, v. 17, p. 797–814.

Bathhurst, R. G., 1975, Carbonate sediments and their diagenesis: New York, Elsevier, 658 p.

Bodnar, R. J., 1990, Petroleum migration in the Miocene Monterey Formation, California, U.S.A.: Constraints from fluid inclusion studies: Mineralogical Magazine, v. 54, p. 295–304.

Boles, J. R., 1998, Carbonate cementation in Tertiary sandstones of the San Joaquin basin, *in* S. Morad, ed., Carbonate cementation in sandstones: International Association of Sedimentology Special Publication 26, p. 261–284.

Boles, J. R., and M. Grivetti, 2000, Calcite cementation along the Refugio/Carneros fault, coastal California: A link between deformation, fluid movement and fluid-rock interaction at a basin margin: Journal of Geochemical Exploration, v. 69–70, p. 313–316.

Boles, J. R., and K. Ramseyer, 1987, Diagenetic carbonate in Miocene sandstone reservoir, San Joaquin basin, California: AAPG Bulletin, v. 71, no. 12, p. 1475–1487.

Boles, J. R., C. A. Landis, and P. Dale, 1985, The Moeraki Boulders— Anatomy of some septarian concretions: Journal of Sedimentary Petrology, v. 55, p. 398–406.

Boles, J. R., J. F. Clark, L. Washburn, and I. Leifer, 2001, Temporal variation in natural methane seep rate due to tides and other factors, Coal Oil Point area, California: Journal of Geophysical Research, v. 106, p. 27,077–27,086.

Budai, J. M., A. M. Martini, L. M. Walter, and T. C. W. Ku, 2002, Fracture-fill calcite as a record of microbial methanogenesis and fluid migration: A case study from the Devonian Antrim Shale, Michigan basin: Geofluids, v. 2, p. 163–183.

Chan, M. A., W. T. Parry, and J. R. Bowman, 2000, Diagenetic hematite and manganese oxides and fault-related fluid flow in Jurassic sandstones, southeastern Utah: AAPG Bulletin, v. 84, p. 1281–1310.

Davatzes, N. C., A. Aydin, and P. Eichhubl, 2003, Overprinting faulting mechanisms during the development of multiple fault sets in sandstone, Chimney Rock fault array, Utah, U.S.A.: Tectonophysics, v. 363, p. 1–18.

DePaolo, D. J., and B. L. Ingram, 1985, High resolution stratigraphy with Sr isotopes: Science, v. 277, p. 938–941.

Dibblee, T. W., 1966, Geology of the central Santa Ynez Mountains, Santa Barbara County, California: California Division of Mines and Geology Bulletin, v. 154, 99 p.

Dibblee, T. W., 1987a, Geologic map of the Goleta Quadrangle: Dibble Geologic Foundation Map DF-07, Santa Barbara, California, scale 1:24,000, 1 sheet.

Dibblee, T. W., 1987b, Geologic map of the Dos Pueblos Quadrangle: Dibble Geologic Foundation Map DF-09, Santa Barbara, California, scale 1:24,000, 1 sheet.

Dibblee, T. W., 1988, Geologic map of the Santa Ynez and Tajiguas quadrangles: Dibble Geologic Foundation Map DF-15, Santa Barbara, California, scale 1:24,000, 1 sheet.

Donovan, T. J., I. Friedman, and J. D. Gleason, 1974, Recognition of petroleum-bearing traps by unusual isotopic composition of carbonate-cemented surface rocks: Geology, v. 2, p. 351–354.

Eichhubl, P., and J. R. Boles, 1998, Vein formation in relation to burial diagenesis in the Miocene Monterey Formation, Arroyo Burro Beach, Santa Barbara, California, *in* P. Eichhubl, ed., Diagenesis, deformation, and fluid flow in the Miocene Monterey Formation: SEPM Pacific Section Special Publication 83, p. 15–36.

Eichhubl, P., and J. R. Boles, 2000a, Focused fluid flow along faults in the Monterey Formation, coastal California: Geological Society of America Bulletin, v. 112, p. 1667–1679.

Eichhubl, P., and J. R. Boles, 2000b, Rates of fluid flow in fault systems— Evidence for episodic rapid fluid flow in the Miocene Monterey Formation, coastal California: American Journal of Science, v. 300, p. 571–600.

Eichhubl, P., H. G. Greene, T. Naehr, and N. Maher, 2000, Structural control of fluid flow: Offshore seepage in the Santa Barbara basin, California: Journal of Geochemical Exploration, v. 69–70, p. 545–549.

Faure, G., 1986, Principles of isotope geology, 2d ed.: New York, John Wiley and Sons, 589 p.

Fischer, P. J., and A. J. Stevenson, 1973, Natural hydrocarbon seeps, Santa Barbara basin, California, *in* P. J. Fisher, ed., Santa Barbara Channel area revisited: AAPG Field Trip Guidebook v. 3, p. 17–28.

Fisher, J. B., and J. R. Boles, 1990, Water-rock interaction in Tertiary sandstones, San Joaquin basin, California, U.S.A.: Diagenetic controls on water composition: Chemical Geology, v. 82, p. 83–101.

Friedman, I., and J. R. O'Neil, 1977, Compilation of stable isotope fractionation factors of geochemical interest, *in* M. Fleischer, ed., Data of geochemistry, 6th ed.: U.S. Geological Survey Professional Paper 440-KK, 12 p.

Gurrola, L. D., A. J. Selting, E. A. Keller, T. Tierney, R. Hartleb, M. Trecker, and T. W. Dibblee, Jr., 2001, Neotectonics of the Santa Barbara fold belt, California, *in* J. Cooper, ed., Geologic excursions in southern California: Field Trip Guidebook and Volume for the Joint Meeting of the Cordilleran Section Geological Society of America and Pacific Section AAPG, April 9–11, 2001, Universal City, California, Fieldtrip Nos. 8–11.

Hathaway, J. C., and E. T. Degens, 1969, Methane-derived marine carbonates of Pleistocene age: Science, v. 165, p. 609–692.

Hayes, M. J., and J. R. Boles, J. R., 1993, Evidence for meteoric recharge in the San Joaquin basin, California, provided by isotope and trace element geochemistry: Marine and Petroleum Geology, v. 10, p. 135–144.

Hornafius, J. S., B. P. Luyendyk, R. R. Terres, and M. J. Kamerling, 1986, Timing and extent of Neogene rotation in the western Transverse Ranges, California: Geological Society of America Bulletin, v. 97, p. 1476–1487.

Hornafius, J. S., D. Quigley, and B. P. Luyendyk, 1999, The world's most spectacular marine hydrocarbon seeps (Coal Oil Point, Santa Barbara Channel, California): Quantification of emissions: Journal of Geophysical Research, v. 104, p. 20,703–20,711.

Ingle, J. C. Jr., 1980, Cenozoic paleobathymetry and depositional history of selected sequences within the southern California continental borderland, *in* W. V. Sliter, ed., Studies in marine micropaleontology and paleoecology; a memorial volume to Orville L. Bandy: Cushman Foundation Special Publication 19, Ithaca, New York, Cushman Foundation for Foraminiferal Research, p. 163–195.

Jackson, P. A., and R. S. Yeats, 1982, Structural evolution of Carpinteria basin, western Transverse Ranges, California: AAPG Bulletin, v. 66, p. 805–829.

Jørgensen, N. O., 1992, Methane-derived carbonate cementation of marine sediments from the Kattegat, Denmark: Geochemical and geologic evidence: Marine Geology, v. 103, p. 1–13.

Kennett, J. P., K. G. Cannariato, I. L. Hendy, and R. J. Behl, 2002, Methane hydrates in Quaternary climate change: The Clathrate gun hypothesis: Washington, D.C., American Geophysical Union, 216 p.

Lee, Y. L., and J. R. Boles, 1996, Depositional control on carbonate cement in the San Joaquin basin, California: Siliciclastic diagenesis and fluid flow: Concepts and applications: SEPM Special Publication 55, p. 13–22.

Losh, S., L. Eglington, P. Schoell, and J. Wood, 1999, Vertical and lateral fluid flow related to a large growth fault, south Eugene Island Block 330, offshore Louisiana: AAPG Bulletin, v. 82, p. 1694–1710.

MacDonald, G. J., 1990, Role of methane clathrates in past and future climates: Climate Change, v. 16, p. 247–281.

Machel, H. G., H. R. Krouse, and R. Sassen, 1995, Products and distinguishing criteria of bacterial and thermochemical sulphate reduction: Applied Geochemistry, v. 10, p. 373–389.

Magoon, L. B, and W. G. Dow, 1994, The petroleum system—From source to trap: AAPG Memoir 60, 644 p.

Martin, J. B., and R. A. Rymerson, 2002, A coupled fluid-inclusion and stable isotope record of paleofluids in the Monterey Formation, California: Geological Society of America Bulletin, v. 114, p. 269–280.

Morad, S., 1998, Carbonate cementation in sandstones: Distribution pattern and geochemical evolution, *in* S. Morad, ed., Carbonate cementation in sandstones: International Association of Sedimentology Special Publication 26, p. 1–26.

Nicholson, C., C. C. Sorlien, T. Atwater, J. C. Crowell, and B. P. Luyendyk, 1994, Microplate capture, rotation of the western Transverse Range, and initiation of the San Andreas transform as a low angle fault system: Geology, v. 22, p. 491–495.

Nisbet, E. G., 1990, Climate change and methane: Nature, v. 347, p. 2001.

Ogle, B. A., W. A. Wallis, R. G. Heck, and E. B. Edwards, 1987, Petroleum geology of the Monterey Formation in the offshore Santa Maria/Santa Barbara areas, *in* R. V. Ingersoll and W. G. Ernst, eds., Cenozoic basin development of coastal California: Engelwood Cliffs, Prentice-Hall, p. 382–406.

Quade, J., T. E. Cerling, and J. R. Bowman, 1989, Systematic variations in the carbon and oxygen isotopic composition of pedogenic carbonate along elevation transects in the southern Great Basin, United States: Geological Society of America Bulletin, v. 101, p. 464–475.

Rademacher, L. K., J. F. Clark, and J. R. Boles, 2003, Groundwater residence times and flow paths in fractured rock determined using environmental tracers in the Mission Tunnel; Santa Barbara County, California, U.S.A.: Environmental Geology, v. 43, p. 557–567.

Raffensperger, J. P., 1996, Numerical simulation of sedimentary basin-scale hydrochemical processes, *in* M. Y. Corapcioglu, ed., Advances in porous media 3: New York, Elsevier, p. 185–305.

Raffensperger, J. P., and G. Garven, 1995, The formation of unconformity-type uranium ore deposits: 2. Coupled hydrochemical modeling: American Journal of Science, v. 295, p. 639–696.

Rohling, E. J., M. Fenton, F. J. Jorissen, P. Bertrand, G. Ganssen, G., and J. P. Caulet, 1998, Magnitudes of sea-level lowstands of the past 500,000 years: Nature, v. 394, p. 162–165.

Sample, J. C., M. R. Reid, H. J. Tobin, and J. C. Moore, 1993, Carbonate cements indicate channeled fluid flow along a zone of vertical faults at the deformation front of the Cascadia accretionary wedge (northwest U.S. coast): Geology, v. 21, p. 507–510.

Schumacher, D., 1996, Hydrocarbon-induced alteration of soils and sediments, *in* D. Schumacher and M. A. Abrams, eds., Hydrocarbon migration and its near-surface expression: AAPG Memoir 66, p. 71–89.

Sibson, R. H., 1994, Crustal stress, faulting, and fluid flow, *in* J. Parnell, ed., Geofluids; origin, migration, and evolution of fluids in sedimentary basins: Geological Society (London) Special Publication 78, p. 69–84.

Tryon, M. D., K. Brown, M. E. Torres, M. Tréhu, J. McManus, and R. W. Collier, 1999, Measurements of transience and downward fluid flow near episodic methane gas vents, Hydrate Ridge, Cascadia: Geology, v. 27, p. 1075–1078.

Whiticar, M. J., and E. Faber, 1986, Methane oxidation in sediment and water column environments— Isotopic evidence, *in* D. Leythaeuser and J. Rulkötter, eds., Advances in organic geochemistry 10: New York, Pergamon Press, p. 759–768.

Wilson, R. D., P. H. Monaghan, A. Osanik, L. C. Price, and M. A. Rogers, 1974, Natural marine oil seepage: Science, v. 184, p. 857–865.

Wilson, A. M., G. Garven, and J. R. Boles, 1999, Paleohydrology of the San Joaquin basin, California: Geological Society of America Bulletin, v. 111, p. 432–449.

Winter, B. L., and L. P. Knauth, 1992, Stable isotope geochemistry of carbonate fracture fills in the Monterey Formation, California: Journal of Sedimentary Petrology, v. 62, p. 208–219.